

A study of the core of the Shapley Concentration: IV. Distribution of intercluster galaxies and supercluster properties [★]

S. Bardelli^{1,2}, E. Zucca¹, G. Zamorani^{1,3}, L. Moscardini⁴ & R. Scaramella⁵

¹ *Osservatorio Astronomico di Bologna, via Ranzani 1, I-40127 Bologna, Italy*

² *Osservatorio Astronomico di Trieste, via Tiepolo 11, I-34131 Trieste, Italy*

³ *Istituto di Radioastronomia del CNR, via Gobetti 101, I-40129 Bologna, Italy*

⁴ *Dipartimento di Astronomia, Università di Padova, vicolo dell'Osservatorio 5, I-35122 Padova, Italy*

⁵ *Osservatorio Astronomico di Roma, via Osservatorio 2, I-00040 Monteporzio Catone (RM), Italy*

E-mail: bardelli@astbo3.bo.astro.it

Received 00 - 00 - 0000; accepted 00 - 00 - 0000

ABSTRACT

We present the results of a redshift survey of intercluster galaxies in the central region of the Shapley Concentration supercluster, aimed at determining the distribution of galaxies in between obvious overdensities. Our sample is formed by 442 new redshifts, mainly in the b_J magnitude range 17 – 18.8. Adding the data from our redshift surveys on the A3558 and A3528 complexes, which are close to the geometrical centre of this supercluster, we obtain a total sample of ~ 2000 radial velocities.

The average velocity of the observed intercluster galaxies in the Shapley Concentration appears to be a function of their (α, δ) position, and it can be fitted by a plane in the three-dimensional space (α, δ, v) : the distribution of the galaxy distances around the best fit plane is described by a Gaussian with dispersion $3.8 \text{ h}^{-1} \text{ Mpc}$.

Using the 1440 galaxies of our total sample in the magnitude range 17 – 18.8, we reconstructed the density profile in the central part of the Shapley Concentration; moreover we detected another significant overdensity at $\sim 30000 \text{ km/s}$ (dubbed S300).

We estimate the total overdensity in galaxies, the mass and the dynamical state of these structures, and discuss the effect of considering a bias between the galaxy distribution and the underlying matter.

The estimated total overdensity in galaxies of these two structures is $(N/\bar{N}) \sim 11.3$ on scale of $10.1 \text{ h}^{-1} \text{ Mpc}$ for the Shapley Concentration and $(N/\bar{N}) \sim 2.9$ on scale of $24.8 \text{ h}^{-1} \text{ Mpc}$ for S300. If light traces the mass distribution, the corresponding masses are $1.4 \times 10^{16} \Omega_o \text{ h}^{-1} M_\odot$ and $5.1 \times 10^{16} \Omega_o \text{ h}^{-1} M_\odot$ for Shapley Concentration and S300, respectively.

A dynamical analysis suggests that, if light traces mass and $\Omega_o = 1$, the Shapley Concentration already reached its turnaround radius and has started to collapse: the final collapse will happen in $\sim 3 \cdot 10^9 \text{ h}^{-1} \text{ yrs}$.

We find an indication that the value of the bias between clusters and galaxies in the Shapley Concentration is higher than that reported in literature, confirming the impression that this supercluster is very rich in clusters.

Finally, from the comparison with some theoretical scenarios, we find that the existence of the Shapley Concentration is more consistent with the predictions of the models with a matter density parameter < 1 , such as open CDM and Λ CDM.

Key words: cosmology: observations – cosmology: large-scale structure of the Universe – galaxies: distances and redshifts – galaxies: clusters: general

1 INTRODUCTION

Superclusters of galaxies are the largest coherent and massive structures known in the Universe. These objects are

[★] based on observations collected at the European Southern Observatory, La Silla, Chile.

crucial in cosmology because their extreme characteristics set topological and physical constraints on the models for galaxy and cluster formation. For this reason, there have been great efforts in order to estimate the extension, shape, mass and dynamical state of these entities.

The most direct way to infer these quantities is to perform a redshift survey in order to map the galaxy distribution in the structure and in its surrounding field, but this method requires a large amount of telescope time and limits the number of targets. Up to now only few of such objects have been studied in detail: the Great Wall (Geller & Huchra 1989; Ramella et al. 1992; Dell’Antonio et al. 1996), the Perseus–Pisces (Haynes & Giovanelli 1986), the Hercules (Barmby & Huchra 1998), and the Corona Borealis (Postman, Geller & Huchra 1988; Small et al. 1998a) superclusters.

Hudson (1993a) computed the mean overdensity of the superclusters found in his redshift compilation ($cz < 8000$ km/s) and estimated that the mean galaxy density excess for these structures is $\sim 3\text{--}5$, on scales of the order of $30\text{--}50$ h^{-1} Mpc (see also Chincarini et al. 1992).

Another way to study superclusters is to detect structures delineated by the distribution of clusters. This method does not require large redshift surveys and relies on the assumption that clusters and galaxies trace in the same way the underlying matter distribution. The Shapley Concentration (Scaramella et al. 1989) stands out as the richest system of Abell clusters of the list of Zucca et al. (1993), at every density excess. In particular, at a density contrast of ~ 2 , it contains 25 members (at mean velocity of ~ 14000 km/s) contained in a box of comoving size ($\alpha \times \delta \times D$) $32 \times 55 \times 100$ h^{-1} Mpc (hereafter $h = H_o/100$). As a comparison, at the same density contrast the Great Attractor, which is the largest mass condensation within 80 h^{-1} Mpc (Lynden–Bell et al. 1988), has only 6 members, while Corona Borealis and Hercules are formed by 10 and 8 clusters, respectively.

Scaramella et al. (1989) suggested that this supercluster could be responsible of a significant fraction of the acceleration acting on the Local Group, by adding its dynamical pull to that of the Great Attractor, which lies approximately in the same direction on the sky at a distance of ~ 4000 km/s. Further studies based on the dipole of the distribution of the Abell clusters (Scaramella et al. 1991, Plionis & Valdarnini 1991) confirmed the suggestion that large scales are important for cosmic flows.

Attempts to determine the density excess and the mass of the Shapley Concentration have been made by Raychaudhury et al. (1991), Scaramella et al. (1994), Quintana et al. (1995) and Ettori et al. (1997): these authors obtained mass estimates of $\sim 10^{16}$ h^{-1} M_\odot . These works are essentially based on estimates of the cluster masses, neglecting the contribution of the intercluster matter. Quintana et al. (1995) gave also a value for the total mass of the supercluster of $\sim 5 \times 10^{16}$ h^{-1} M_\odot on a scale of ~ 17 h^{-1} Mpc, using the virial mass estimator applied to the distribution of clusters. They computed the velocity dispersion and the virial radius using the mean velocity and the bi-dimensional positions of clusters: this result could be biased if the physical elongation along the line of sight of the supercluster is not negligible.

Studying the cluster distribution, at high density contrast the Shapley Concentration is characterized by three dense complexes of interacting clusters, dominated by

A3558, A3528 and A3571, respectively. At lower density contrast these three systems connect to each other through a large cloud of clusters. The clusters in the A3558 and A3528 complexes appear to be aligned perpendicularly to the line of sight and approximately at the same distance, thus suggesting the presence of an elongated underlying structure. However, when the whole supercluster is considered, it appears to be extended along the line of sight (see e.g. figure 4 in Tully et al. 1992 and Zucca et al. 1993).

The distribution of clusters inside this supercluster is quite well studied; on the contrary, little is known about the distribution of the intercluster galaxies. Very recently, Drinkwater et al. (1999) performed a redshift survey limited to the magnitude $R < 16$ in the southern central part of the Shapley Concentration, finding evidences of sheets of galaxies connecting the clusters.

The study of the properties of intercluster galaxies is very important in order to assess the physical reality and extension of the structure and to determine if galaxies and clusters trace the matter distribution in the same way. In this context, we are carrying on a long term multiwavelength study of the central part of the Shapley Concentration, studying both cluster and intercluster galaxies. In this paper we present the results of an intercluster galaxy redshift survey, from which we obtained ~ 450 new velocity determinations, and the analysis of the whole supercluster properties.

The plan of the paper is the following: in Sect. 2 we describe the results of the intercluster galaxy survey and in Sect. 3 we present the characteristics of the cluster galaxy samples. In Sect. 4 we analyze the galaxy distribution and in Sect. 5 we describe the methods adopted to recover the density profile and the mass of the whole structure. In Sect. 6 we derive the overdensities associated to intercluster and cluster galaxies, we estimate the mass of the supercluster and its dynamical state and we discuss our results. Finally in Sect. 7 we provide the summary. In the following, the values $H_o = 100$ km/s Mpc $^{-1}$ and $q_o = 0.5$ will be adopted.

2 THE INTERCLUSTER GALAXY SAMPLE

As pointed out above, the Shapley Concentration is very rich in clusters with respect to the other known structures. The aim of the intercluster survey is therefore to study how the galaxies trace this supercluster and which percentage of the mass of the supercluster lies outside the clusters.

2.1 The catalogue

Figures 1a, b, c show the isodensity contours for the galaxies in the b_J magnitude range $17\text{--}19.5$ from the COSMOS/UKST galaxy catalogue (Yentis et al. 1992) in the three plates 443, 444 and 509, which cover the central part of the Shapley Concentration.

In order to check the existence of possible zero point photometric errors in our data, we compared the COSMOS magnitudes with the CCD sequences of Cunow et al. (1997), available for plates 443 and 444. After having applied the correction for the non-linearity of the COSMOS magnitude scale proposed by Lumsden et al. (1997), we found $\langle b_J - B_{CCD} \rangle \sim -0.02 \pm 0.06$ mag using 12

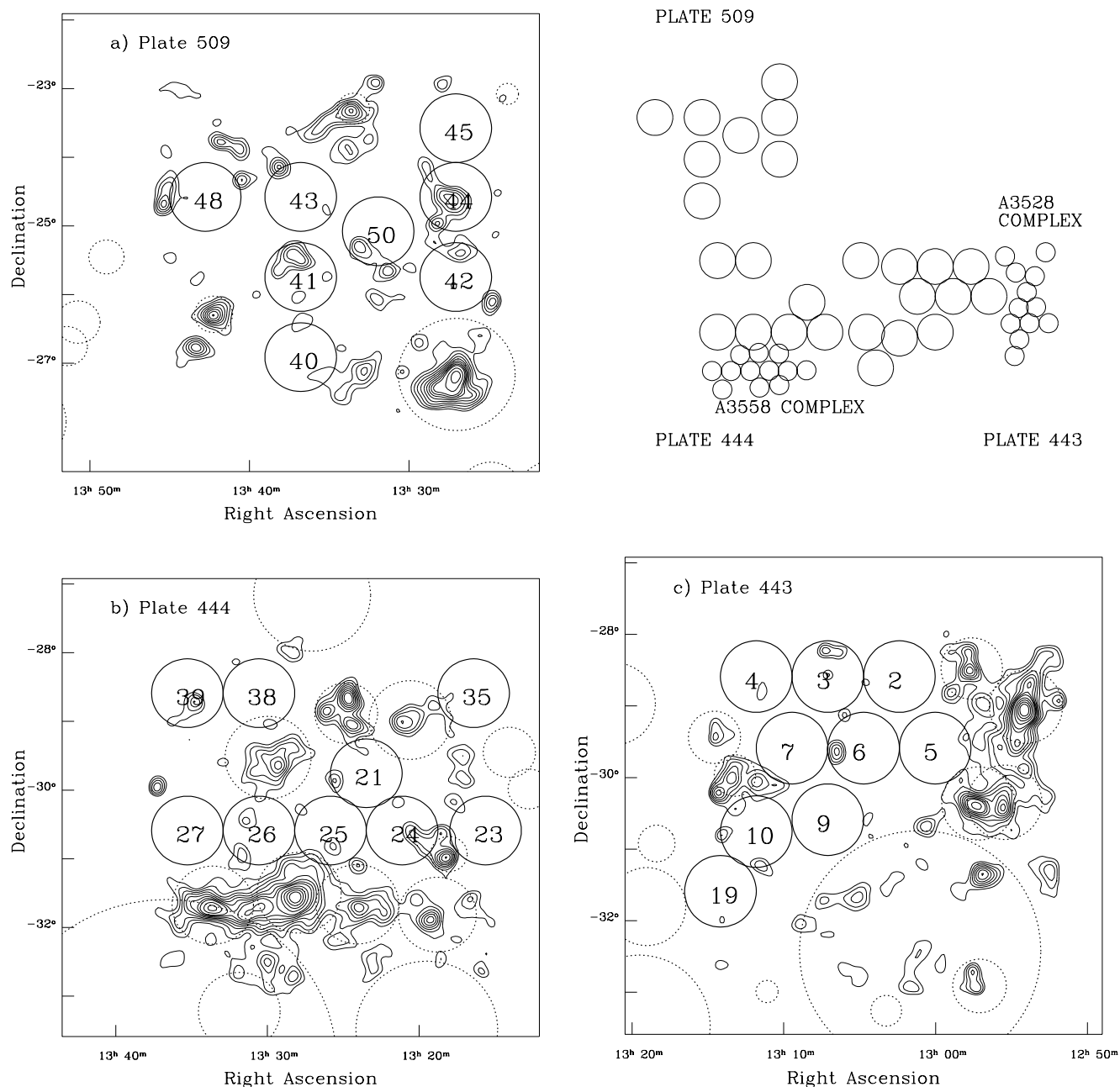


Figure 1. Isodensity contours of the bidimensional distribution of the galaxies in the b_J magnitude bin 17 – 19.5 in the UKSTJ plates which cover the central part of the Shapley Concentration. The data have been binned in 2×2 arcmin pixels and then smoothed with a Gaussian with a FWHM of 6 arcmin. For the Abell clusters present in the plates, circles of one Abell radius have been drawn (dashed curves). Solid circles represent the MEFOS fields.

a) Plate 509; b) Plate 444; c) Plate 443. The two most evident systems are the A3558 (plate 444) and the A3528 (plate 443) cluster complexes. The dashed circle at the bottom right corner of plate 509 corresponds to the cluster A1736. The relative positions of the fields is shown in the upper right panel, where small circles represent observations on the cluster complexes.

galaxies in the b_J range 16 – 18.4. Since no CCD sequences are available for plate 509, we checked its photometric zero point using the galaxies in the region overlapping the adjacent plate 444, finding that the two magnitude scales are in agreement. We also checked the photometric zero point for ESP survey galaxies (Vettolani et al. 1997), which represent our “field” normalization (see Sect.5.1), using the CCD

sequences of Cunow (1993). We found, using 13 galaxies, $\langle b_J - B_{CCD} \rangle \sim -0.03 \pm 0.09$ mag. These results show, on one side, that there is no systematic zero point shift in the photometric scale of our plates; on the other side, they confirm the consistency of our data with respect to the ESP data, which we will use as normalization in the overdensity estimates (see Sect.5.1).

Finally, we found that a color correction for the conversion from b_J to B_{CD} magnitudes is not required: this fact was already noted analysing independent CCD sequences on ESP galaxies (Garilli et al., in preparation).

The data in Figure 1 have been binned in 2×2 arcmin pixels and then smoothed with a Gaussian with a FWHM of 6 arcmin. For the Abell clusters present in the plates, circles of one Abell radius have been drawn (dashed circles). The magnitude range of galaxies in the figure has been chosen in order to enhance the features at distances equal to or greater than that of the Shapley Concentration. In fact, at 14500 km/s the apparent magnitude of an M^* galaxy is ~ 16.2 .

The solid circles in Figure 1 correspond to the field of view of the multifiber spectrograph MEFOS (one degree of diameter, ~ 0.785 square degrees), which carries the fibers on rigid arms and allows the contemporary observation of 29 galaxies. This number would match the galaxy density in the b_J magnitude range 17–18.2: unfortunately, due to the constraints which avoid arm collisions, only part of the objects are observable. Therefore, in order not to waste fibers, we have chosen to extend the magnitude range to 17.0–18.8: in this range, the average number of galaxies per field is ~ 70 .

In Table 1 we report the coordinates of the centre and the relative UKSTJ plate of the 26 observed fields. Note that in choosing the pointing directions, we avoided clusters, in order to observe mainly true “field” objects, to which hereafter we refer as intercluster galaxies.

In the upper right panel of Figure 1 the relative positions of the observed fields are shown, together with the positions (small circles) of the observed fields on the cluster complexes (see Sect. 3).

2.2 Observations and data reduction

Spectroscopic observations were performed at the 3.6m ESO telescope at La Silla, equipped with the MEFOS multifiber spectrograph (Bellenger et al. 1991; Felenbok et al. 1997) in the nights of 8-9-10 April 1994. The MEFOS multifiber spectrograph was mounted at the prime focus of the telescope and allowed the contemporary observation of 29 scientific targets. Each fiber, whose projected diameter on the sky is ~ 2.6 arcsec, was coupled with another one devoted to a simultaneous sky observation. This has in principle two advantages: the sky spectrum is measured very nearby the considered galaxy and the exposure is taken at the same time. Moreover, after having checked that background spatial variations are not present, it is possible to average the 29 sky spectra in order to obtain a “mean” sky with an enhanced signal-to-noise ratio.

As pointed out in Bardelli et al. (1994), the sky subtraction procedure in fiber spectroscopy requires the determination of the relative fiber transmissions, which we estimated on the basis of the $[\text{OI}]\lambda 5577$ sky line. MEFOS allowed also the possibility of “beam-switching”, i.e. the change between the object and the nearby sky fiber. Dividing the observation in two exposures and applying this option, galaxy and sky fall on the same fiber in different moments: this would allow a direct subtraction of the sky from the galaxy spectrum. However, even if this procedure avoids the problems given by the fiber-to-fiber different transmission, it can fail to correctly subtract the sky when the latter changes significantly

Table 1. Centres of the observed MEFOS fields

Field	α (2000)	δ (2000)	# Plate
2	13 02 27	-28 36 00	443
3	13 07 00	-28 36 00	443
4	13 11 38	-28 36 00	443
5	13 00 07	-29 36 00	443
6	13 04 44	-29 36 00	443
7	13 09 21	-29 36 00	443
9	13 07 04	-30 36 00	443
10	13 11 43	-30 46 00	443
19	13 14 04	-31 36 00	443
21	13 23 34	-29 45 21	444
23	13 15 49	-30 35 21	444
24	13 21 14	-30 35 21	444
25	13 25 52	-30 35 21	444
26	13 30 30	-30 35 21	444
27	13 35 09	-30 35 21	444
35	13 16 42	-28 35 21	444
38	13 30 29	-28 35 21	444
39	13 35 04	-28 35 21	444
40	13 36 47	-26 54 37	509
41	13 36 47	-25 44 37	509
42	13 27 11	-25 44 37	509
43	13 36 47	-24 34 37	509
44	13 27 14	-24 34 37	509
45	13 27 16	-23 34 37	509
48	13 42 40	-24 34 37	509
50	13 32 00	-25 04 37	509

between the two exposures. We found that this happened at large zenithal angles or at the beginning and at the end of the night. However, we used both methods and we always considered the procedure which gives the higher number of measured radial velocities in each field.

The spectra, obtained with a CCD TEK512 CB and the ESO grating #15, have a resolution of $\sim 12 \text{ \AA}$ and a pixel size of $\sim 4.6 \text{ \AA}$. They were cross-correlated with a set of 8 stellar and 8 galaxy templates using the XCSAO program of Kurtz et al. (1992). For spectra showing emission lines, we used the EMSAO program in the same package. Details of the reductions and the cross-correlation are given in Bardelli et al. (1994).

2.3 The redshift sample

We observed a total of 685 objects, instead of the maximum number of 754 in principle allowed by the number of fibers (29×26 fields), due to collision constraints in the robotic arms of the MEFOS spectrograph. Among these 685 spectra, 85 were not useful for a redshift determination (12% of the total), due to a poor signal to noise ratio. Among the 600 good spectra, 158 objects resulted to be stars (26% of the total), leaving us with 442 galaxy velocities.

In Table 2, we list the galaxies with velocity determination. Columns (1), (2) and (3) give the right ascension (J2000), the declination (J2000) and the b_J apparent magnitude of the object, respectively. Columns (4) and (5) give the heliocentric velocity ($v = cz$) and the internal cross correlation error: this value has to be multiplied by a factor 1.6-1.9 in order to find the true statistical error (see Bardelli et al.

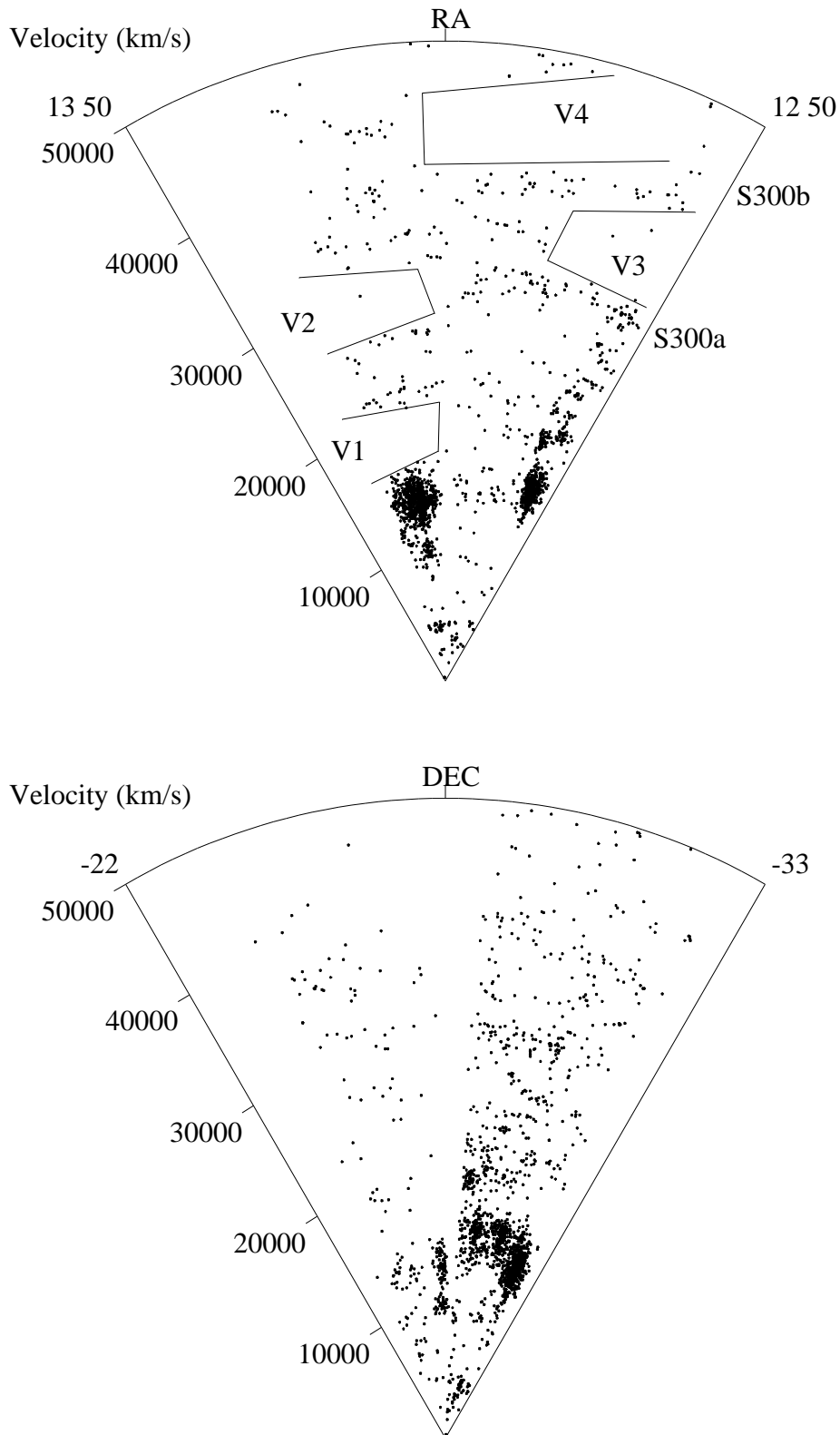


Figure 2. Wedge diagram of the galaxy distribution in our samples. Upper panel: 1728 galaxies in the plates 444 and 443 and in the velocity range [0 – 50000] km/s. Note the clear presence of the A3558 and A3528 complexes and of four voids (see text for details). Lower panel: 1979 galaxies in plates 443, 444 and 509 in the velocity range [0-50000] km/s. Note that the plotted coordinate is the declination.

1994). The code “emiss” in column (6) denotes the velocities obtained from emission lines.

Finally in the following analysis we included also 69 velocities found in the literature (not reported in Table 2) for objects in our surveyed region and therefore our total sample has 511 velocities. The average redshift completeness of the sample in the magnitude range 17 – 18.8 is $\sim 25\%$.

3 THE CLUSTER GALAXY SAMPLE

3.1 The A3558 cluster complex

Figure 1b clearly shows the presence on the plate 444 of an elongated structure formed by the ACO clusters A3558, A3562 and A3556, which is located at the geometrical centre of the Shapley Concentration. This complex has been extensively studied in the optical (Bardelli et al. 1994, 1998a, 1998b), in the X-ray (Bardelli et al. 1996) and in the radio (Venturi et al. 1997, 1998) wavelengths. We found that this structure may be a cluster-cluster collision seen just after the first core-core encounter. In order to determine the excess in number of galaxies, we used the redshift sample presented in Bardelli et al. (1998a), consisting of 714 velocities over an area of $3^\circ.12 \times 1^\circ.4$, to which we added the 60 new redshifts published by the ENACS survey (Katgert et al. 1998). In order to maximize the completeness, we restricted our analysis to the well sampled region corresponding to the OPTOPUS fields (see Bardelli et al. 1998a), covering an area of about 2.7 square degrees. In this sample, there are 723 galaxies with velocity determination, out of a total of 1582 ($\sim 46\%$) to the limit $b_J = 19.5$. Restricting the sample in the magnitude range 17 – 18.8, the completeness is $\sim 64\%$ (456/711).

3.2 The A3528 cluster complex

Another remarkable cluster complex is found at the westernmost part of plate 443 (Figure 1c) and is formed by the ACO clusters A3528, A3530 and A3532. We performed a redshift survey in this structure with the OPTOPUS multi-fibre spectrograph, obtaining 581 new velocities in an area of $3^\circ.38 \times 1^\circ.72$, including also the cluster A3535 (Bardelli et al., in preparation). After a search in the literature, we found 79 additional velocities from Quintana et al. (1995) and ENACS (Katgert et al. 1998), leading to a final sample of 660 redshifts. As done for the A3558 complex, we restricted the sample to the area sampled by the 12 OPTOPUS fields (about 2.7 square degrees). In this area the completeness is $\sim 46\%$ (645/1399) to $b_J = 19.5$ and $\sim 72\%$ (475/656) in the magnitude range 17 – 18.8.

3.3 Other clusters

In the region under consideration, in addition to the clusters cited above, there are several other Abell/ACO clusters. Among them, A3537 and A3565 are part of the Great Attractor, while A1736, A3554, A3555, A3559 and A3560 are members of the main structure of the Shapley Concentration. The cluster A3552, westward of A3556, was not previously included in this supercluster by Zucca et al. (1993) because of the value of its estimated redshift: now the available redshifts for this cluster (Quintana et al. 1995) put it

in the distance range of the Shapley Concentration. An ambiguous case is that of A3557, which has two velocity peaks: only one of them is compatible with the supercluster.

Among the remaining clusters, A1757, A1771, A3540, A3546 and A3551 may belong to another structure at 30000 km/s (S300, see below). Finally the clusters A3531 and A3549 are at intermediate distance between Shapley Concentration and S300, while A1727 and A3544 are more distant objects, on the basis of their estimated redshifts.

Among the clusters which are part of the Shapley Concentration, the only one which has been sampled enough to be useful in our analysis is A1736, clearly visible in the lower right corner of plate 509 (Figure 1a). The redshifts in A1736 have been taken by Dressler & Shectmann (1988) and Stein (1996), and the final sample contains 111 velocities (54 in the magnitude range 17 – 18.8). For the others, the redshift data found in the literature are too sparse to allow density reconstructions, therefore we choose to neglect these clusters. We ignore also the more distant clusters, because of the lack of data. Therefore, all the following results for the Shapley Concentration and S300 have to be regarded as *lower limits* for what concerns the cluster contribution.

4 ANALYSIS OF THE GALAXY DISTRIBUTION

The total velocity sample we used contains 2057 velocities. In Figure 2a, we plot the wedge diagram of the galaxies with redshifts in the plates 444 and 443. The two cluster complexes dominated by A3558 (on the left) and by A3528 (on the right) are clearly visible: these two structures appear to be connected by a bridge of galaxies, similar to the Coma-A1367 system, the central part of the Great Wall. The scale of this system is $\sim 23 \text{ h}^{-1} \text{ Mpc}$ and it is comparable to that of Coma-A1367 ($\sim 21 \text{ h}^{-1} \text{ Mpc}$). Note the presence of two voids at $\sim 20000 \text{ km/s}$ and $\sim 30000 \text{ km/s}$ in the easternmost half of the wedge, labelled as V1 and V2 respectively. Other two voids (V3 and V4) are visible in the westernmost part of the plot: in particular, void V3 appears to be delimited by two elongated features (S300a and S300b) which appear to “converge” in a single feature at right ascension $\sim 13^h$ (S300c). We refer to this structure with the name S300: as shown below, the overdensity corresponding to this excess is remarkably high, even if it is not clear if all these features are part of a single structure.

Figure 2b shows the distribution of all the galaxies (plates 443, 444 and 509) of the sample in the velocity range [0 – 50000] km/s. Note that the plotted sky coordinate is the declination. The apparent “hole” in the galaxy distribution in the middle of the wedge ($\delta \sim 27^\circ$) is due to a poor sampling of the southern part of plate 509 and to the fact that the literature data for A1736 are less deep than those in our survey.

4.1 The structure of the Shapley Concentration

The average velocity of the observed intercluster galaxies appears to be a function of the (α, δ) position, ranging from 12289 km/s for the galaxies in plate 509 to 15863 km/s for the galaxies in plate 443. This fact was also noted by Quintana et al. (1995) as a relationship between the cluster

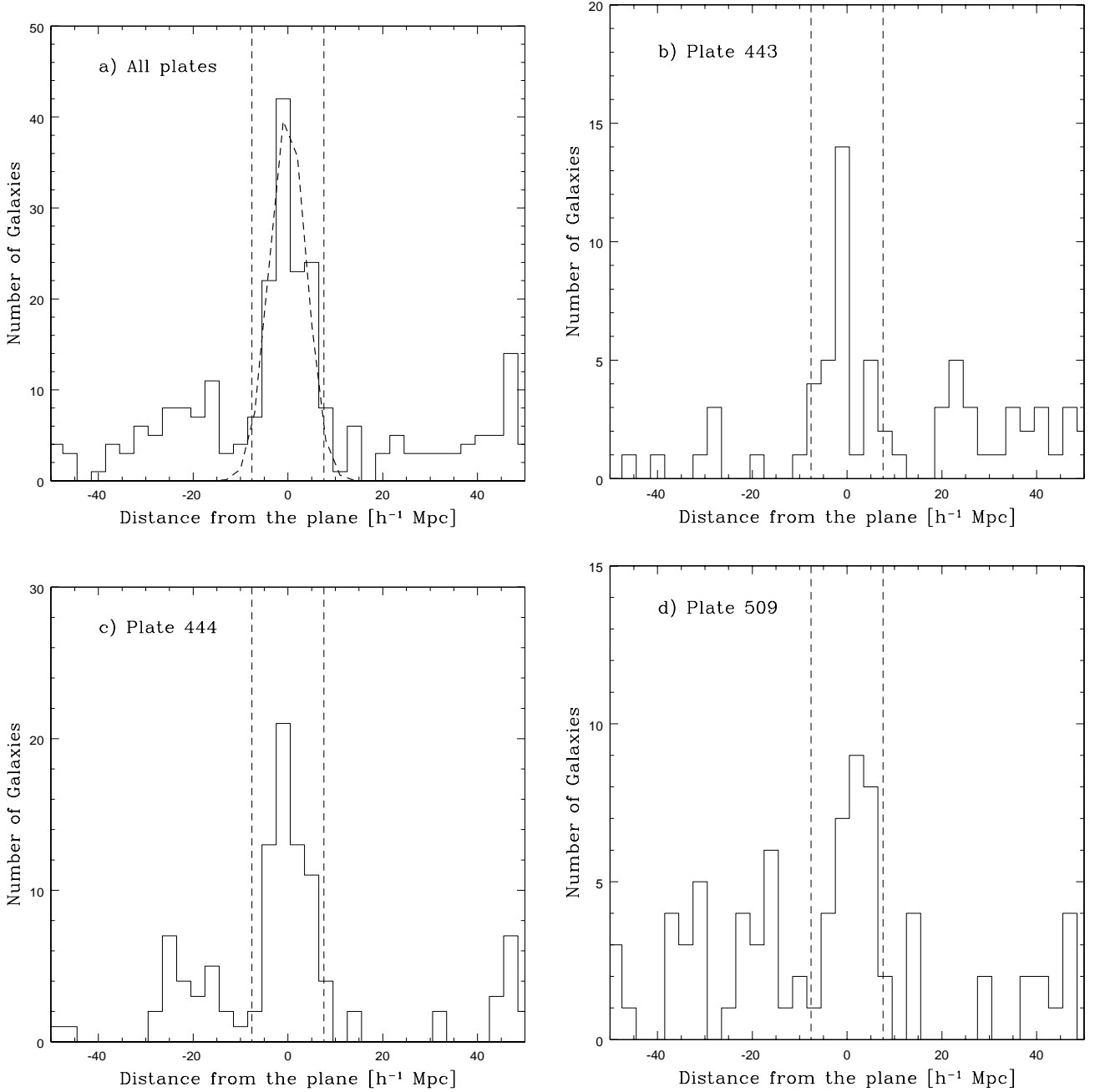


Figure 3. Histograms of the distances from the fitted plane for all galaxies in the intercluster survey (panel a) and for galaxies in each plate (panels b, c, d). The vertical dashed lines indicate the interval assumed for the estimate of the supercluster overdensity. In the upper left panel the fitted Gaussian with $\sigma = 3.8 \text{ h}^{-1} \text{ Mpc}$ is drawn.

radial velocities and the right ascension. Inspection of the trend of the average velocity as a function of position suggests that it can be reasonably described by a plane in the three-dimensional space (α, δ, v) :

$$a(x - x_m) + b(y - y_m) + c(z - z_m) = 0, \quad (1)$$

where

$$x = \frac{v}{100} \cos(\delta - \delta_m) \sin(\alpha - \alpha_m) \text{ h}^{-1} \text{ Mpc}$$

$$y = \frac{v}{100} \sin(\delta - \delta_m) \text{ h}^{-1} \text{ Mpc}$$

$$z = \frac{v}{100} \cos(\delta - \delta_m) \cos(\alpha - \alpha_m) \text{ h}^{-1} \text{ Mpc}$$

and the subscript m indicates the average value of the variable.

Each galaxy has a distance from the plane

$$d = \frac{a(x - x_m) + b(y - y_m) + c(z - z_m)}{\sqrt{a^2 + b^2 + c^2}} \text{ h}^{-1} \text{ Mpc}. \quad (2)$$

Minimizing the sum of the squared distances of galaxies from the plane, we find

$$a = 0.9 \quad b = 1.4 \quad c = 1.1. \quad (3)$$

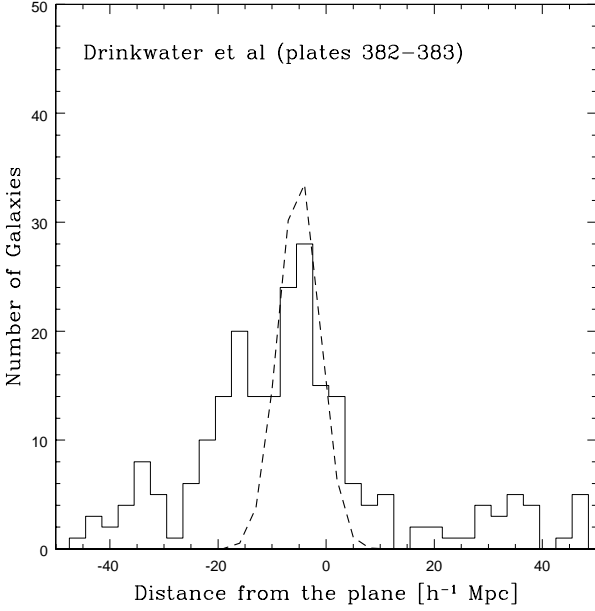


Figure 4. Histogram of the distances from the plane of the galaxies in Plates 382 and 383 from the Drinkwater et al. (1999) survey. Superimposed is the Gaussian with $\sigma = 3.8 \text{ h}^{-1} \text{ Mpc}$ and a mean distance of $-5.0 \text{ h}^{-1} \text{ Mpc}$.

In Figure 3 we show the histograms of the distances from the fitted plane. In panel a) the distribution of distances of the whole intercluster sample is shown: the peak corresponding to the Shapley Concentration is clearly visible. The secondary bump at $d \sim -20 \text{ h}^{-1} \text{ Mpc}$ corresponds to the structure at $\sim 11000 \text{ km/s}$ found by Drinkwater et al. (1999). This plane, which describes the ridge of the distribution of the galaxies, is a reasonably good fit over the entire extension of our survey, as shown by the distance histograms of galaxies divided in the three surveyed plates (Figure 3b, c, d).

A Gaussian fit to the distribution of the distances around the best fit plane gives a dispersion $\sigma = 3.8 \text{ h}^{-1} \text{ Mpc}$. This dispersion is significantly narrower than what would be obtained ($\sigma_{vel} = 1011 \text{ km/s}$) by fitting a Gaussian to the velocity distribution of the galaxies in the same region.

We checked also if this representation of the galaxy distribution holds outside our surveyed region using the velocity sample of Drinkwater et al. (1999), which covers plate 444 and two southern adjacent plates (382 and 383). Although the plane parametrization seems correct, we find a shift in the mean of $\sim -5 \text{ h}^{-1} \text{ Mpc}$ in the plates 382 and 383. In Figure 4 we show the histogram of the distances from the plane of galaxies in plates 382 and 383.

In Figures 3a and 4 the fitted Gaussian is superimposed to the histograms. Note that in Figure 4 the mean has been shifted by $-5.0 \text{ h}^{-1} \text{ Mpc}$.

5 DENSITY EXCESSES AND MASSES

5.1 The density excess estimate

In order to estimate the overdensity associated to each structure and to reconstruct the density-distance profile, it is necessary to determine the number of galaxies expected in the case of a uniform distribution, under the same observational constraints (i.e. with the same redshift incompleteness), and the volume occupied by each structure.

The first step is the determination of the selection function of the survey. For each sample, we computed the expected number of galaxies in the case of uniform distribution as

$$N(z)dz = \sum_i C(m_i) \int_{L_{min}(m_i, z)}^{L_{max}(m_i, z)} \phi(L) \frac{dV}{dz} dL dz, \quad (4)$$

where V is the volume, $L_{min}(m_i, z)$ and $L_{max}(m_i, z)$ are the minimum and maximum luminosity seen in the sample at the redshift z , given the apparent magnitude limits of the sample. The quantity $C(m_i)$ represents the incompleteness of the survey, i.e. the ratio between the number of galaxies with redshifts and the total number of objects, as a function of the apparent magnitude, and

$$\phi(L)dL = \phi^* \left(\frac{L}{L^*} \right)^\alpha e^{-L/L^*} d \left(\frac{L}{L^*} \right) \quad (5)$$

is the luminosity function of field galaxies parametrized with a Schechter (1976) function. We adopted the values $\alpha = -1.22$, $M^* = -19.61$ and $\phi^* = 0.02$ found by Zucca et al. (1997) for the ESP survey, which uses our same photometric catalogue. We applied the correction for the non-linearity of the COSMOS magnitude scale proposed by Lumsden et al. (1997) and the extinction values of Burstein & Heiles (1984). The intercluster sample has been obtained in the magnitude range $17-18.8$ and for consistency we limited also the other samples in the same magnitude range.

The upper panels of Figures 5 and the left upper panel of 6 show the histograms of the galaxies in the cluster and intercluster samples, with superimposed the distribution expected for the corresponding uniform sample. The lower panels of the same figures show the overdensity $\frac{N}{\bar{N}}$ as a function of the comoving distance, where N is the observed number of galaxies and \bar{N} is the number of objects expected in the volume occupied by the structure in the case of uniform distribution. The plotted errors represent Poissonian uncertainties in the observed galaxy counts and a dotted line corresponding to $\frac{N}{\bar{N}} = 1$ has been drawn as a reference.

The second step is the estimate of the volume occupied by the structure under consideration. While the solid angle is assumed to be given by the surveyed area, the determination of the width of the supercluster in the direction along the line of sight is more subjective. The data in the cluster complexes can not be used for this determination, because of the presence of significant peculiar velocities due to the virialization of clusters (also known as “finger-of-God” effect), which broaden the width in the velocity space. Therefore, we estimated the width of the supercluster by using only the distribution of galaxies in the intercluster survey, where the peculiar velocities are expected to be significantly smaller. Since we find that the distribution of the distances from the best fit plane of the intercluster galaxies in the Shapley Concentration can be reasonably well described by a Gaussian

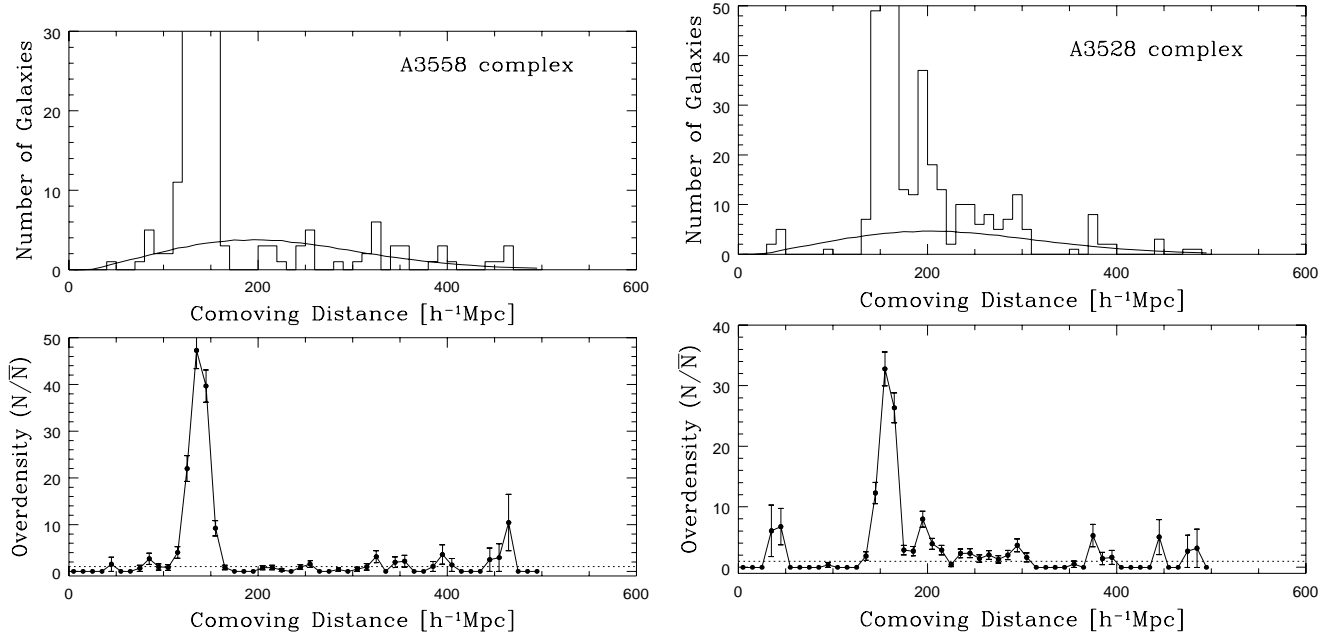


Figure 5. Upper panels: Histograms of the velocities in the A3558 (left) and A3528 (right) complexes with superimposed the distribution expected for a uniform sample. Note that the histograms have been truncated on the Y-axis in order to better show the distribution of field galaxies: in the central peak there are ~ 150 galaxies for A3558 and ~ 140 galaxies for A3528. Lower panels: Galaxy density profiles. The dotted line corresponds to $\frac{N}{\bar{N}} = 1$. The errors are computed assuming Poissonian fluctuations of the number of detected objects in the considered bin.

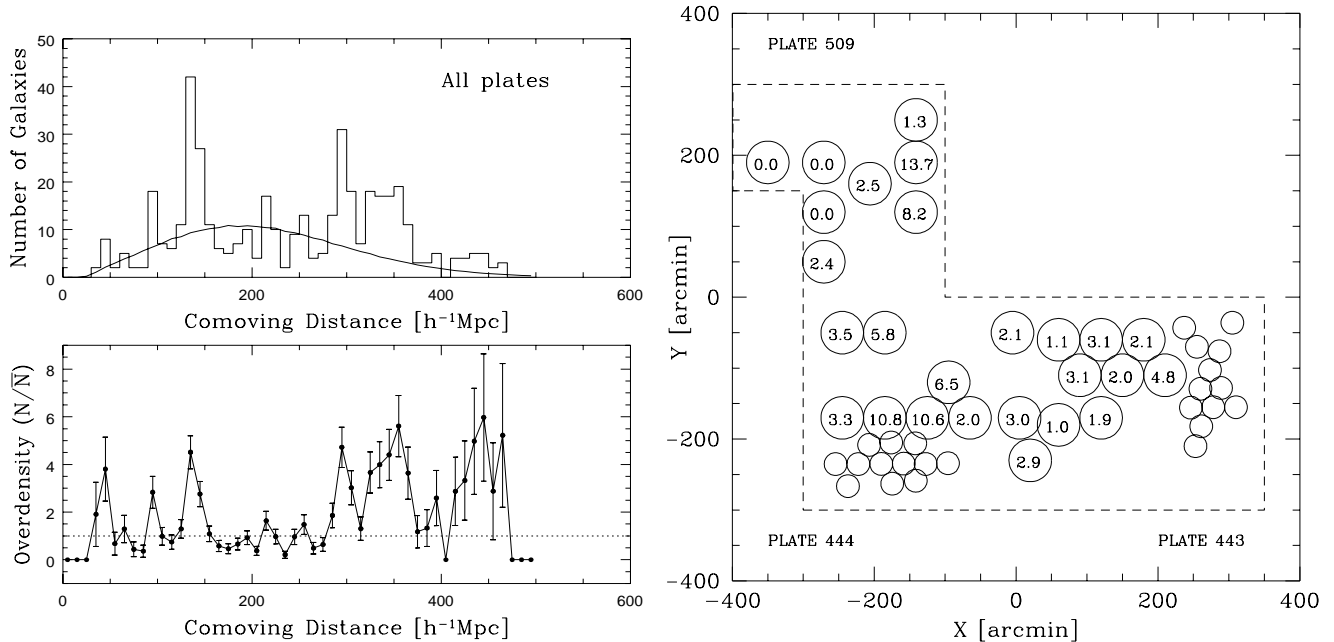


Figure 6. Left panel: Same as Figure 5 for the intercluster galaxies sample. Right panel: estimated overdensities in the single MEFOS fields as distributed in the sky.

function (see previous Section), we considered as part of the supercluster all galaxies with distance from the plane smaller than $\pm 2\sigma$. Since the plane is tilted with respect to the (α, δ, v) reference frame, this choice produces a variable velocity range depending on the position. The minimum and maximum velocity ranges are $\Delta v \sim 2400$ km/s and $\Delta v \sim 3100$ km/s for fields #48 (plate 509) and #5 (plate 443), respectively.

The physical width is assumed to be simply $\Delta v/H_o$, a choice acceptable in the case of low peculiar velocities. It is impossible to have an estimate of the peculiar velocity pattern of this region, because of the difficulty of modelling the mass distribution: however, since it is reasonable to think that this region (except the clusters) is not yet virialized, we expect that galaxies are still infalling toward the centre of the structure. We could parametrize this uncertainty as done by Small et al. (1998a), which introduced the parameter F , defined as the ratio between the width of the supercluster in redshift space and in real space. In this case

$$\left(\frac{N}{N}\right)_{real} = F \left(\frac{N}{N}\right)_{obs}.$$

If the peculiar infall velocities (perpendicular to our fitted plane) were of the order of ~ 150 km/s, similar to those measured in the Great Wall (Dell'Antonio, Geller & Bothun 1996), the value of F for our structure would be ~ 0.83 , so that our derived overdensities could be overestimated by $\sim 17\%$. Given the uncertainties on the amount of peculiar velocities, in the following we prefer to present our results neglecting the effect of F .

Also in the cluster complexes and in A1736 we assumed that the width of the supercluster is the same as that derived from our fit of the intercluster galaxies, even if, due to the high peculiar motions induced by the virialized state of these clusters, these structures appear significantly elongated in redshift space. In order to correct, at least partially, for this effect, we applied the following procedure. First we assigned to the supercluster all objects with distance $\pm 2\sigma$ from the fitted plane; then we considered galaxies outside this velocity range: when they were in excess with respect to the expected number, we assigned them to the supercluster.

We note that this procedure is somewhat arbitrary, in particular in presence of substructures infalling toward the clusters with high velocity. In the density profile plots these substructures may appear as secondary peaks clearly separated by the main overdensity. In these cases, it is impossible to say if the observed difference in velocity between the main and secondary peaks is due to a real spatial distance (and in this case it would be not correct to assign galaxies of the substructure to the supercluster) or to a velocity difference. In our sample there are two clear cases of this kind. In the A3528 complex, there is the clump corresponding to A3535 at $v \sim 20000$ km/s, while in the A1736 cluster we find the substructure already detected by Dressler & Shectman (1988). In order to derive a conservative estimate of the supercluster overdensity, we choose to neglect these sub-clumps.

The definition of the limits of S300 is not very clear, because on plate 443 it consists of two features (see Figure 2a), well separated by a void (labelled V3), while on plates 444 and 509 appears as a single feature. In the plate 443 sample, the nearest peak (S300a) appears to extend from 28000 to 31000

km/s, while the velocity range of the farthest (S300b) overdensity is [34000 – 38000] km/s. In the plate 444 and 509 samples, S300 appears as a single density excess (S300c): we estimate a velocity range of [30000 – 37000] km/s for the plate 444 sample and [32000 – 35000] km/s for the plate 509 sample.

It is not clear if all these features are part of a single structure, but on the other hand the distribution of galaxies in this region appears highly coherent. For this reason, we computed a global overdensity in this region, regardless of the physical association among the various components: therefore, in the following we will present the results obtained considering the sum of the contributions of S300a, S300b, V3 and S300c.

The third step is the computation of the overdensity $\frac{N}{N}$ for each structure. The total overdensity in galaxies can then be estimated by combining the density excesses of the various samples following Postman, Geller & Huchra (1988) as

$$\left(\frac{N}{N}\right)_{SC} = \sum_i f_i \left(\frac{N}{N}\right)_i, \quad (6)$$

where f_i is the volume fraction occupied by the considered i^{th} sample with overdensity $\left(\frac{N}{N}\right)_i$.

In Table 3 the overdensities of the single structures (listed in column 1) and the total density excess in the Shapley Concentration are reported in column 2. The volumes and the redshift completeness of the samples are also reported (column 3 and 6). In Table 4 we present the estimated overdensities and the volumes involved in the S300 samples.

In order to assign a formal scale to these overdensities, we calculated the radius of each structure assuming a spherical shape as

$$R = \left(\frac{3V}{4\pi}\right)^{\frac{1}{3}}, \quad (7)$$

where R is the scale and V is the volume. In column 4 of Tables 3 and 4, the values of the scale for each structure in the various samples are reported.

5.2 The mass estimate

A direct measure of the mass in the supercluster regions between clusters is not possible, because their small overdensities indicate that they are far from virialization. For this reason we use the number excess in galaxies, which can be related to the mass excess (see below).

For what concerns the clusters, in previous studies from the literature their contribution to the total mass or overdensity has been derived by adding together the results of the virial mass estimates of each cluster. In order to be fully consistent with the density excess derived for the intercluster survey, we chose to estimate also the cluster contribution as an excess in galaxy number. This procedure could be incorrect if there is a significant segregation between visible and dark matter in clusters with respect to the field, i.e. the proportionality between light and mass is different inside and outside clusters. However, the peculiar dynamical situation of the clusters in this region could also influence the reliability of the mass estimates. Indeed, there is not agreement

Table 3. Estimated overdensities for the samples in the Shapley Concentration

Sample	Overdensity $\frac{N}{\bar{N}}$	Volume [h ⁻³ Mpc ³]	Scale [h ⁻¹ Mpc]	Mass [Ω_o h ⁻¹ M _⊙]	Redshift completeness
A3558 complex	46.4 ± 2.4	415.6	4.6	5.4 10 ¹⁵	64%
A3528 complex	21.4 ± 1.2	609.5	5.3	3.6 10 ¹⁵	72%
A1736	19.7 ± 3.1	247.8	3.9	1.4 10 ¹⁵	22%
Intercluster sample	3.9 ± 0.4	3082.8	9.0	3.3 10 ¹⁵	25%
Total sample	11.3 ± 0.4	4355.8	10.1	1.4 10 ¹⁶	41%
Extended sample	6.8 ± 0.4	11611.3	14.1	2.2 10 ¹⁶	
Extended sample+382&383	5.2 ± 0.3	15607.8	15.5	2.3 10 ¹⁶	

Table 4. Estimated overdensities in the S300 structure

Sample	Overdensity $\frac{N}{\bar{N}}$	Volume [h ⁻³ Mpc ³]	Scale [h ⁻¹ Mpc]	Mass [Ω_o h ⁻¹ M _⊙]
S300a	4.5 ± 0.6	7760.1	12.3	9.8 10 ¹⁵
V3 void	0.0	12506.4	14.4	0.0
S300b	3.8 ± 0.7	14806.7	15.2	1.6 10 ¹⁶
S300c	3.2 ± 0.4	28783.2	19.0	2.6 10 ¹⁶
Total	2.9 ± 0.3	63856.4	24.8	5.1 10 ¹⁶

even for the mass of A3558, the richest and best studied cluster of the Shapley Concentration. The mass obtained from optical data ranges from $3.4 \times 10^{14} \text{ h}^{-1} \text{ M}_{\odot}$ (Dantas et al. 1997) to $6 \times 10^{14} \text{ h}^{-1} \text{ M}_{\odot}$ (Biviano et al. 1993), while the X-ray data give masses in the range $1.5 - 6.0 \times 10^{14} \text{ h}^{-1} \text{ M}_{\odot}$ (Bardelli et al. 1996, Ettori et al. 1997).

We remind also that in the overdensity estimates we neglected the contribution of a number of clusters (see Sect. 3.3), for which the available data are too sparse for a density reconstruction. However, having rescaled the overdensity found for A1736 with the ratio of the ACO richness parameters of these clusters, we found that neglecting their contribution to the total overdensity of the Shapley Concentration leads to an underestimate of $\frac{N}{\bar{N}}$ of the order of 10%.

Given the volume and the overdensity of a structure, the mass can be estimated as

$$M = 2.778 \times 10^{11} \left(\frac{N}{\bar{N}} \right) V \Omega_o \text{ h}^{-1} \text{ M}_{\odot} , \quad (8)$$

where V is the volume (in $\text{h}^{-3} \text{ Mpc}^3$) occupied by the considered structure, $\frac{N}{\bar{N}}$ is its number excess in galaxies with respect to a uniform distribution and Ω_o is the matter density parameter. This relation is correct only if the luminous matter traces exactly the distribution of the total matter. The values found for the masses of the various structures by using eq.(8) are reported in column 5 of Table 3 and Table 4.

As a more general case, we can assume (following Kaiser 1994) that the density excess in galaxies (or in clusters) is proportional to the total mass overdensity through the bias factor b

$$\frac{N - \bar{N}}{\bar{N}} = b \left(\frac{\rho - \bar{\rho}}{\bar{\rho}} \right) . \quad (9)$$

Hudson (1993a, 1993b), comparing the peculiar velocity field in the local Universe with the distribution of optical galaxies, estimated the most likely range for the bias factor to be approximately $2.5\Omega_o^{0.6} - 1.4\Omega_o^{0.6}$. The first value comes from the comparison of the overdensity of the Virgo supercluster with the Virgo infall pattern, while the second value is obtained by assuming that the large-scale galaxy dipole converges at a depth of 8000 km/s. Therefore, the lower value could be an underestimate of b if the dipole of the peculiar velocities has a deeper depth (Plionis & Valdarnini 1991; Scaramella et al. 1991). Indeed, an analysis of the dipole component perpendicular to the supergalactic plane led to the higher value of $2.0\Omega_o^{0.6}$ (Hudson 1993a).

6 RESULTS AND DISCUSSION

The total overdensity of the Shapley Concentration in our surveyed region, computed following eq.(6), is $\frac{N}{\bar{N}} = 11.3$ over a scale of $10.1 \text{ h}^{-1} \text{ Mpc}$ (see Table 3). In order to give an idea of the spatial pattern of the galaxy overdensity inside the Shapley Concentration, in the right panel of Figure 6 we give the value of $\frac{N}{\bar{N}}$ in each MEFOS field: as expected, these values are higher in proximity of the clusters. In the North-East part the overdensities decrease and there are three fields with no observed galaxies in the considered velocity range: note however that since the expected number of galaxies in these fields is ~ 0.8 , fields with no galaxies are still compatible with the mean density. Field # 44 has the highest overdensity value (13.7), probably because of the

presence of a group.

If we assume that the estimated overdensity of the intercluster galaxies extends also outside the MEFOS fields over the region covered by plates 443, 444 and 509 (see the area delimited by dashed lines in Figure 6), the total galaxy excess derived from eq.(6) is 6.8 ± 0.4 on a scale of $14.1 \text{ h}^{-1} \text{ Mpc}$. Hereafter we refer to this case as “extended sample”, while with the name “total sample” we indicate the results for our original surveyed area. We remind that these samples include the contribution of the A3528 and A3558 complexes and of A1736, but neglect the contribution of the other clusters in the region (see Sect.3.3): therefore these overdensity values have to be regarded as lower limits.

Drinkwater et al. (1999) give a value of $\frac{N}{\bar{N}} = 2.0 \pm 0.2$ for plates 382 and 383, over an area of 44 sq.deg.; in order to add the contribution of this survey to our data, we computed its volume in the following way. As shown in Figure 4, our plane representation holds also in this sample; for the width determination we assume that this plane is perpendicular to the line of sight, therefore we adopt a width of $\pm 7.6 \text{ h}^{-1} \text{ Mpc}$ (see Sect.4.1). We added the contribution of these plates to our sample, following eq.(6). With these values we find for the Shapley Concentration a total overdensity of $\frac{N}{\bar{N}} = 5.2 \pm 0.3$ on a scale of $15.5 \text{ h}^{-1} \text{ Mpc}$. Hereafter we refer to this case as “extended sample + 382 & 383”. Also in this case, given the fact that the contribution of clusters in plates 382 and 383 has been neglected, the overdensity values are lower limits.

For what concerns the S300 structure, we have a total overdensity of $\frac{N}{\bar{N}} = 2.9$ over a scale of $24.8 \text{ h}^{-1} \text{ Mpc}$: in Table 4 the various contributions to this structure are reported. However, we remark that it is not clear if all these features are physically part of a single structure: for this reason the values of the reported overdensities have to be regarded as indicative of the matter distribution in this region.

Given these overdensities, the total mass of the Shapley Concentration in our surveyed region and of the S300 structure are $1.4 \times 10^{16} \Omega_o \text{ h}^{-1} \text{ M}_\odot$ and $5.1 \times 10^{16} \Omega_o \text{ h}^{-1} \text{ M}_\odot$, respectively, if light traces mass.

The contribution of the Shapley Concentration to the peculiar velocity of the Local Group with respect to the Cosmic Microwave Background reference frame could be estimated as (Davis & Peebles 1983)

$$\Delta v = 2.86 \cdot 10^{-7} \frac{\Delta M}{v^2} \Omega_o^{-0.4} \text{ h km/s}, \quad (10)$$

where ΔM is the mass excess (in M_\odot) of the structure with respect to a uniform distribution and v is the mean radial velocity (in km/s).

Considering the “extended + 382 & 383” sample, we find $\Delta v \sim 26 \text{ km/s}$ (for $\Omega_o = 1$ and no bias): note however that this value corresponds only to the central part of the Shapley Concentration and does not take into account the contribution of the matter in the external regions of the supercluster.

As a comparison, the peculiar velocity induced on the Local Group by the Great Attractor is predicted to be of the order of $\sim 300 \text{ km/s}$ by Hudson (1993a).

Finally, it is possible to study how clusters and galaxies trace the same structure. Assuming a mean cluster den-

sity of 25.2×10^{-6} clusters Mpc^{-3} (as found by Zucca et al. 1993 for the ACO clusters), we expect in the surveyed region of the Shapley Concentration (delimited by the dashed lines in Figure 6) 0.29 clusters, to be compared with the 11 observed. This corresponds to an overdensity in clusters of $\left(\frac{N}{\bar{N}}\right)_{cl} = 37.9 \pm 11.4$. The quantity

$$b_{cl,g} = \left[\left(\frac{N}{\bar{N}}\right)_{cl} - 1 \right] / \left[\left(\frac{N}{\bar{N}}\right)_{gal} - 1 \right]$$

represents the ratio between the bias factors of clusters and galaxies. We found $b_{cl,g} = 6.4 \pm 2.0$ on a scale of $14.1 \text{ h}^{-1} \text{ Mpc}$. Although the large associated error, this quantity seems to be inconsistent with the range of 2–3.5 found for $b_{cl,g}$ comparing the dipoles (Branchini & Plionis 1996) or the ratio of the correlation functions (see Scaramella et al. 1994) or the reconstructed linear power spectra (Peacock & Dodds 1994) of the distribution of clusters and galaxies. As reference, the same quantity for the Corona Borealis supercluster is $b_{cl,g} = \frac{7.53}{7} \sim 1$ on $\sim 20 \text{ h}^{-1} \text{ Mpc}$, where the value for the galaxies is taken from Small, Sargent & Hamilton (1998b). This fact, while is confirming the impression that the Shapley Concentration has an anomalous richness in clusters with respect to other superclusters, on the other hand could raise problems for a simple comparison between results on the large-scale distribution of clusters and galaxies, because suggests significant variations of $b_{cl,g}$ with the local density. However, in order to assess this result, detailed studies of the galaxy distribution in a sample of superclusters are needed and are now possible with the new generation of multi-objects facilities.

6.1 Comparison with previous results

The comparison of our values for Shapley Concentration and S300 with the results from the literature for other superclusters is not straightforward, because of the different scales over which the overdensities are computed. Moreover, sometimes the density excesses are given in *mass*, sometimes in *number* of galaxies or clusters, therefore a direct comparison needs hypotheses about the value of Ω_o and of the bias factor b . Moreover, these comparisons are affected by the relatively large uncertainties in the estimated values. However, it can be instructive to compare the results obtained using different methods to estimate masses and overdensities, as f.i. virial masses, X-ray masses, etc.

The overdensity for the Shapley Concentration (extended sample + 382&383) can be compared with the density excess in *mass* given by Raychaudhury (1989) for the Great Attractor on a similar scale ($\frac{\rho}{\bar{\rho}} = 6\Omega_o^{-1}$ over $15 \text{ h}^{-1} \text{ Mpc}$). Under the hypothesis that $\Omega_o = 1$ and that the galaxy distribution traces that of the total matter, the two superclusters would be very similar on the considered scale.

A more consistent comparison can be done with the list of superclusters of Hudson (1993a), who studied the distribution of optical galaxies taken from the UGC and ESO-Uppsala catalogues within 8000 km/s. On scales comparable with those considered in our survey for the Shapley Concentration, only the overdensities of the Virgo (Local)supercluster and the Fornax-Eridanus supercluster have been determined (see his table 10), finding $\frac{N}{\bar{N}} = 2.70$ and 1.35, respectively. Comparisons with the other structures

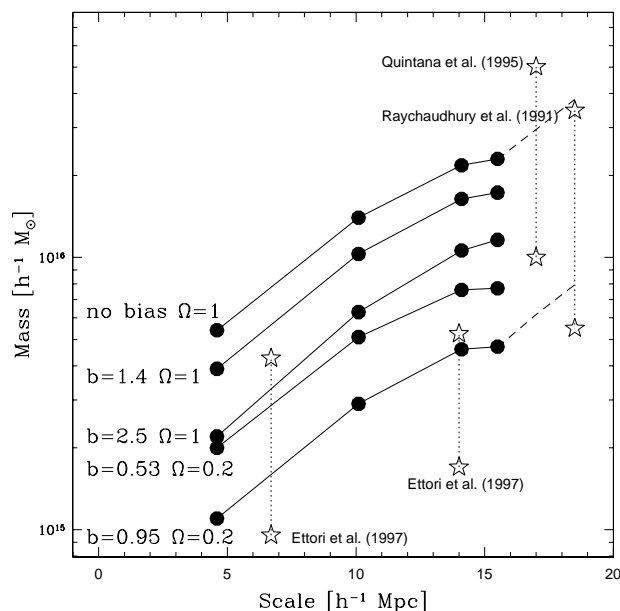


Figure 7. Estimated masses at various scales for different parameter choices, indicated near each curve. Stars connected with dotted lines refer to mass ranges given in the literature. Dashed lines give the extrapolation of our mass values to the scales of Quintana et al. and Raychaudhury et al., assuming the same overdensity we found at our largest scale.

of Hudson (1993a), which are considered at very different scales, are not straightforward: indeed, as can be noticed from Tables 3 and 4, there are large variations of $\frac{N}{\bar{N}}$ inside superclusters when different scales are considered.

The value of $\frac{N}{\bar{N}} = 3.1$ for the overdensity in *galaxies* in the Great Attractor on a scale of $\sim 30 \text{ h}^{-1} \text{ Mpc}$ (Dressler 1988) can be compared with the value of ~ 2.9 of S300, revealing the similarity of these two structures. Note, however, that our value is a lower limit since we neglected the presence of clusters in the S300 structure.

Marinoni et al. (1998), fitting the galaxy peculiar velocity field from the MarkIII catalogue (Willick et al. 1997) and the spiral galaxy sample of Matthewson, Ford & Buchhorn (1992) with a multi-attractor model, found for the Shapley Concentration $\frac{\rho - \bar{\rho}}{\bar{\rho}} \sim 2.7$ and 3.8 , respectively, within a scale of $15 \text{ h}^{-1} \text{ Mpc}$: the comparison with our $\frac{N}{\bar{N}}$ for the “extended + 382& 383” sample leads to values for the bias factor of $b \sim 1.6$ and 1.1 , consistent with the adopted range of Hudson (1993a, 1993b). Note that Marinoni et al. (1998) used a model with spherical symmetry, while the geometry of our sample is much more complicated: however, if we use the Marinoni’s values obtained for scales of $10 \text{ h}^{-1} \text{ Mpc}$ and $20 \text{ h}^{-1} \text{ Mpc}$, the estimates for b do not significantly change. These results mean that the value of the bias factor inside the Shapley Concentration does not differ from those found in other regions of the local Universe.

Adopting the Hudson’s values for the bias parameter, the mass of the Shapley Concentration in our surveyed re-

gion results in the range $[6.3 - 10.3] \times 10^{15} \text{ h}^{-1} \text{ M}_\odot$ in the case of $\Omega_o = 1$ and $[2.9 - 5.1] \times 10^{15} \text{ h}^{-1} \text{ M}_\odot$ in the case of $\Omega_o = 0.2$. The relative overdensity ranges are $\frac{\rho - \bar{\rho}}{\bar{\rho}} = [4.1 - 7.4]$ and $[10.8 - 19.4]$, respectively. The mass values for each scale and for different choices of b and Ω_o are shown in Figure 7.

The mass of the Shapley Concentration can be compared with other estimates found in the literature, also shown in Figure 7. Raychaudhury et al. (1991), using the virial mass estimator, found $M_{vir} = 3.5 \times 10^{16} \text{ h}^{-1} \text{ M}_\odot$ on scales of $18.5 \text{ h}^{-1} \text{ Mpc}$, and simply summing the cluster masses found $M = 5.5 \times 10^{15} \text{ h}^{-1} \text{ M}_\odot$ on the same scale. This range is consistent with the more recent estimates of Quintana et al. (1995) on a scale of $17 \text{ h}^{-1} \text{ Mpc}$: also for these authors, the higher mass value is derived with the virial estimator and the lower one is the sum of cluster masses. These values can be compared with the mass we derived considering the “extended sample + 382 & 383” discussed above for the Shapley Concentration, that is $2.3 \times 10^{16} \Omega_o \text{ h}^{-1} \text{ M}_\odot$ on a scale of $15.5 \text{ h}^{-1} \text{ Mpc}$ (with no bias). Assuming that the overdensity derived for this sample can be extended also to larger scales, we extrapolated the expected mass values at the Quintana et al. and Raychaudhury et al. scales in the two extreme cases for b and Ω_o : these extrapolations are shown as dashed lines in Figure 7. Our mass range is compatible with both the Quintana et al. and the Raychaudhury et al. values. However note that our estimate at the scale $15.5 \text{ h}^{-1} \text{ Mpc}$ has to be regarded as a lower limit, because does not include the contribution of all clusters in the region.

On a scale of $\sim 14 \text{ h}^{-1} \text{ Mpc}$ Ettori et al. (1997), using various mass estimators, found values in the range $[1.7 - 5.2] \times 10^{15} \text{ h}^{-1} \text{ M}_\odot$. This range is consistent only with our lower estimate for the “extended sample” on scale $14.1 \text{ h}^{-1} \text{ Mpc}$: however, these authors took into account only the clusters, neglecting the contribution of matter outside clusters.

Ettori et al. (1997) gave a mass estimate also for the core of the supercluster, ranging from $1.0 \times 10^{15} \text{ h}^{-1} \text{ M}_\odot$ to $4.3 \times 10^{15} \text{ h}^{-1} \text{ M}_\odot$ on a scale of $6.7 \text{ h}^{-1} \text{ Mpc}$. On a comparable scale ($4.6 \text{ h}^{-1} \text{ Mpc}$ on the A3558 complex), we find values in the range $[2.2 - 3.9] \times 10^{15} \text{ h}^{-1} \text{ M}_\odot$ in the case of bias and $\Omega_o = 1$ and $[1.1 - 2.0] \times 10^{15} \text{ h}^{-1} \text{ M}_\odot$ in the case of bias and $\Omega_o = 0.2$. The relative overdensity ranges are $\frac{\rho - \bar{\rho}}{\bar{\rho}} = [18.2 - 32.4]$ and $[47.8 - 85.7]$, respectively, to be compared with the range $[4.05 - 11.47]$ given by Ettori et al. (1997). Also in this case, the discrepancy between these ranges is probably due to the fact that these authors neglected the contribution of the matter outside clusters on the considered scale.

6.2 Dynamics and comparison with theoretical models

Rich superclusters are ideal laboratories where to study all the dynamical phenomena like cluster formation, because the high local densities induce high peculiar velocities, which accelerate merging events. A standard method to study the dynamical state of our structures is to follow the evolution of their equivalent present linear overdensities (Kaiser & Davis 1985; see Appendix A of Ettori et al. 1997 for the details of

Table 5. Dynamical state of the structures

Sample	Linear Overdensity $\frac{N}{\bar{N}}$	Linear scale [h ⁻¹ Mpc]	Turnaround Time [10 ⁹ h ⁻¹ yrs]	Collapse Time [10 ⁹ h ⁻¹ yrs]
A3558 complex	2.5	15.8	3.8	7.7
A3528 complex	2.4	13.9	4.3	8.5
Shapley Concentration	2.3	21.6	4.9	9.8
S300 structure	1.8	32.1	10.1	20.2

the formalism). In practice, the linear overdensity and scale are the values that a structure would have if its gravitational evolution were linear.

In Table 5 we report the values of the linear density excess (column (2)), linear radius (column (3)) and turnaround and collapse times (columns (4) and (5)) in the case of $\Omega_o = 1$ and no bias for the various structures (indicated in column (1)). The times have to be compared with the age of the Universe, which is $t_o = 6.5 \cdot 10^9$ h⁻¹ yrs (in the Einstein-deSitter case).

From the values in Table 5 it is clear that, if light traces mass and $\Omega_o = 1$, the Shapley Concentration already reached its turnaround radius and started to collapse: the final collapse will happen in $\sim 3 \cdot 10^9$ h⁻¹ yrs. We computed the turnaround times also in the case of high and low bias ($b = 2.5\Omega_o^{0.6}$ and $b = 1.4\Omega_o^{0.6}$ respectively) and $\Omega_o = 1$ and $\Omega_o = 0.2$, finding that the Shapley Concentration is still following a decelerated expansion in all cases, except in the case of low bias and $\Omega_o = 1$, for which the structure has just started to collapse.

For what concerns the S300 structure, it results it is well far from the collapse in all considered scenarios.

The dynamical analysis of the cluster complexes indicates that the A3558 complex is at the late stages of the collapse, which will happen in $\sim 1 \cdot 10^9$ h⁻¹ yrs. This result is consistent with the analysis of the A3558 complex by Bardelli et al. (1994, 1998a, 1998b), who found a complex dynamical situation, related to cluster mergings. Analogous results about the A3528 complex will be presented in Bardelli et al. (in preparation).

Having calculated the linear scale and overdensity of the structures, it is possible to compare them with the predictions of various theoretical models. We considered a set of six different cosmological models belonging to the general class of Cold Dark Matter (CDM) scenarios (see e.g. Moscardini et al. 1998):

- 1) the standard CDM model, with a normalization consistent with the COBE data (SCDM_{COBE});
- 2) the same model but with a different normalization, in agreement with the cluster abundances (SCDM_{CL});
- 3) the so-called τ CDM model with a shape parameter $\Gamma = 0.21$;
- 4) a tilted CDM model with $n = 0.8$ (TCDM);
- 5) an open CDM model with a matter density parameter $\Omega_o = 0.2$ (OCDM);
- 6) a low density ($\Omega_o = 0.2$) CDM model with flatness given by the cosmological constant (Λ CDM).

All these models, except the first, are normalized by using the observed cluster abundance (see Eke, Cole & Frenk

1996). Note that this normalization is also compatible with the COBE normalization, with the exception of SCDM_{CL}, for which this normalization gives predicted values $\sim 43\%$ higher. For this reason, we present the results for SCDM with both COBE and cluster normalizations.

In Table 6 we report the ratio between the linear overdensity and the r.m.s. mass fluctuations predicted by the various models for the “total” sample and with different choices of Ω_o and b ; the results for the “extended” and “extended + 382&383” samples are similar.

In order to assess the statistical consistency of the Shapley Concentration “event” with the predictions of the models, it is necessary to calculate how many of such structures are expected in the sampled volume of the Universe. Our survey is not useful to this purpose, because it covers a small solid angle just in the direction of the Shapley Concentration. Therefore, we decided to consider the cluster sample used by Zucca et al. (1993) to search for superclusters: this sample covers the whole sky with $|b^{\text{II}}| > 15^\circ$ up to a distance of ~ 300 h⁻¹ Mpc. In this volume there are no other superclusters as rich as the Shapley Concentration. We computed the ratio between this volume and the volume of our samples listed in Table 3: this corresponds to the number of available “probes”. Given this number, it is possible to estimate the number of σ over which only 0.25 objects are expected in a Gaussian distribution. This number of σ is 4.33 for the “total” sample. If the ratio between the linear overdensity and the r.m.s. mass fluctuations predicted by the various models exceeds this number of σ , we expect to have no event like the Shapley Concentration in the sampled volume.

Therefore the existence of the Shapley Concentration is inconsistent with all models in Table 6 which predict values higher than ~ 4 ; the consistent values are written in italic in Table 6. The most discrepant model is the SCDM_{CL}; the TCDM and τ CDM give marginally consistent values only in case of high bias. On the contrary, all models with a matter density parameter < 1 seem to be compatible with the existence of a Shapley Concentration “event”. Finally, note that the SCDM_{COBE} appears to give the lowest values, but this model is inconsistent with other results obtained on the scales of galaxies and clusters (see e.g. Peacock & Dodds 1996).

7 SUMMARY

We have presented the results of a redshift survey of intercluster galaxies toward the central part of the Shapley

Table 6. Comparison with theoretical models

	SCDM _{COBE}	SCDM _{CL}	τ CDM	TCDM	OCDM	Λ CDM
Shapley Concentration total sample						
$\Omega_o = 1$ no bias	3.07	7.22	5.79	6.49		
$\Omega_o = 1$ $b = 1.4$	2.54	5.96	4.90	5.43		
$\Omega_o = 1$ $b = 2.5$	1.81	4.26	3.63	3.93		
$\Omega_o = 0.2$ no bias					2.79	2.58
$\Omega_o = 0.2$ $b = 0.53$					3.73	3.43
$\Omega_o = 0.2$ $b = 0.95$					2.86	2.63

Concentration supercluster, aimed at determining the distribution of galaxies in between obvious overdensities. Our sample is formed by 442 new redshifts mainly in the b_J magnitude range 17 – 18.8. Together with our redshift surveys on the A3558 and A3528 complexes, our total sample has ~ 2000 velocities.

Our main results are the following:

- The average velocity of the observed intercluster galaxies in the Shapley Concentration appears to be a function of the (α, δ) position, and can be fitted by a plane in the three-dimensional space (α, δ, v) : the distribution of the galaxy distances around the best fit plane is described by a Gaussian with a dispersion of $3.8 \text{ h}^{-1} \text{ Mpc}$.
- Using the 1440 galaxies of our sample in the magnitude range 17 – 18.8, we reconstructed the density profile in the central part of the Shapley Concentration and we detected another significant overdensity at $\sim 30000 \text{ km/s}$ (dubbed S300).
- We estimated the total overdensity in galaxies, the mass and the dynamical state of these structures, discussing the effect of considering a bias between the galaxy distribution and the underlying matter. The estimated total overdensity in galaxies of these two structures is $\frac{N}{\bar{N}} \sim 11.3$ on scale of $10.1 \text{ h}^{-1} \text{ Mpc}$ for the Shapley Concentration and $\frac{N}{\bar{N}} \sim 2.9$ on scale of $24.8 \text{ h}^{-1} \text{ Mpc}$ for S300. If light traces the mass distribution, the corresponding masses are $1.4 \times 10^{16} \Omega_o \text{ h}^{-1} M_\odot$ and $5.1 \times 10^{16} \Omega_o \text{ h}^{-1} M_\odot$ for Shapley Concentration and S300, respectively.
- The dynamical analysis revealed that, if light traces mass and $\Omega_o = 1$, the Shapley Concentration already reached its turnaround radius and started to collapse: the final collapse will happen in $\sim 3 \text{ 10}^9 \text{ h}^{-1} \text{ yrs}$.
- We compared our mass estimates on various scales with other results in the literature, finding a general agreement.
- We found an indication that the value of the bias between clusters and galaxies in the Shapley Concentration is higher than that reported in literature, confirming the impression that this supercluster is very rich in clusters.
- Finally from the comparison with some theoretical scenarios, we found that the Shapley Concentration is more consistent with the predictions of the models with a matter density parameter < 1 , such as open CDM and Λ CDM.

ACKNOWLEDGEMENTS

We warmly thank Andrea Biviano for having given us an electronic version of the redshift data on A1736 and Christian Marinoni for his overdensity data of the Shapley Concentration.

REFERENCES

- Bardelli S., Zucca E., Vettolani G., Zamorani G., Scaramella R., Collins C.A., MacGillivray H.T., 1994, MNRAS 267, 665
- Bardelli S., Zucca E., Malizia A., Zamorani G., Scaramella R., Vettolani G., 1996, A&A 305, 435
- Bardelli S., Zucca E., Zamorani G., Vettolani G., Scaramella R., 1998a, MNRAS 296, 599
- Bardelli S., Pisani A., Ramella M., Zucca E., Zamorani G., 1998b, MNRAS 300, 589
- Barmby P., Huchra J.P., 1998, AJ 115, 6
- Bellenger R., Dreux M., Felenbok P., Fernandez A., Guerin J., Schmidt R., Avila G., D’Odorico S., Eckert W., Rupprecht G., 1991, The Messenger 65, 54
- Biviano A., Girardi M., Giuricin G., Mardirossian F., Mezzetti M., 1993, ApJ 411, L13
- Branchini E., Plionis M., 1996, ApJ 460, 569
- Burstein D., Heiles C., 1984, ApJSS 54, 33
- Chincarini G., Guzzo L., Scaramella R., Vettolani G., Iovino A., 1992, in Fabian A.C. ed, Clusters and Superclusters of Galaxies, Kluwer, Dordrecht, p. 253
- Cunow B., 1993, A&ASS 97, 541
- Cunow B., Duemmler R., Spiekermann G., Ungruhe R., Wargau W.F., 1997, A&ASS 125, 71
- Dantas C.C., de Carvalho R.R., Capelato H. V., Mazure A., 1997, ApJ 485, 447
- Davis M., Peebles P.J.E., 1983, ARAA 21, 109
- Dell’Antonio I.P., Geller M.J., Bothun G.D., 1996, AJ 112, 1780
- Dressler A., 1988, ApJ 329, 519
- Dressler A., Shectman S.A., 1988, AJ 95, 985
- Drinkwater M.J., Proust D., Parker Q.A., Quintana H., Slezak E., 1999, PASA in press
- Eke V.R., Cole S., Frenk C.S., 1996, MNRAS 282, 263
- Ettori S., Fabian A.C., White D.A., 1997, MNRAS 289, 787
- Felenbok P., Guerin J., Fernandez A., Cayatte V., Balkowski C., Kraan-Korteweg R.C., 1997, Experimental Astronomy 7, 65
- Geller M.J., Huchra J.P., 1989, Science 246, 897
- Haynes M., Giovanelli R., 1986, ApJ 306, 155
- Hudson M.J., 1993a, MNRAS 265, 43
- Hudson M.J., 1993b, MNRAS 265, 72
- Kaiser N., 1984, ApJ 284, L9
- Kaiser N., Davis M., 1985, ApJ 297, 365

Katgert P., Mazure A., den Hartog R., Adami C., Biviano A., Perea J., 1998, *A&ASS* 129, 399

Kurtz M.J., Mink D.J., Wyatt W.F., Fabricant D.G., Torres G., Kriss G.A., Tonry J.L., 1992, in Worrall D.M., Biemesderfer C., Barnes J. eds, *Astronomical Data Analysis Software and Systems I*, ASP conference series vol.25, p.432

Lumsden S.L., Collins C.A., Nichol R.C., Eke V.R., Guzzo L., 1997, *MNRAS* 290, 119

Lynden-Bell D., Faber S.M., Burstein D., Davies R.L., Dressler A., Terlevich R.J., Wegner G., 1988, *ApJ* 326, 19

Marinoni C., Monaco P., Giuricin G., Costantini B., 1998, *ApJ* 505, 484

Matthewson D.S., Ford V.L., Buchhorn M., 1992, *ApJS* 81, 413

Moscardini L., Coles P., Lucchin F., Matarrese S., 1998, *MNRAS* 299, 95

Peacock J.A., Dodds S.J., 1994, *MNRAS* 267, 1020

Peacock J.A., Dodds S.J., 1996, *MNRAS* 280, L19

Plionis M., Valdarnini R., 1991, *MNRAS* 249, 46

Postman M., Geller M.J., Huchra J.P., 1988, *AJ* 281, 95

Quintana H., Ramirez A., Melnick J., Raychaudhury S., Szelak E., 1995, *AJ* 110, 463

Ramella M., Geller M.J., Huchra J.P., 1992, *ApJ* 384, 396

Raychaudhury S., 1989, *Nature* 342, 251

Raychaudhury S., Fabian A.C., Edge A.C., Jones C., Forman W., 1991, *MNRAS* 248, 101

Scaramella R., Baiesi-Pillastrini G., Chincarini G., Vettolani G., Zamorani G., 1989, *Nature* 338, 1562

Scaramella R., Vettolani G., Zamorani G., 1991, *ApJ* 376, L1

Scaramella R., Vettolani G., Zamorani G., 1994, *ApJ* 422, 1

Schechter P., 1976, *ApJ* 203, 297

Small T.A., Ma C., Sargent W.L., Hamilton D., 1998a, *AJ* 492, 45

Small T.A., Sargent W.L., Hamilton D., 1998b, in Hamilton D. ed., *The Evolving Universe*, Kluwer, Dordrecht, p.155

Stein P., 1996, *A&ASS* 116, 203

Tully R.B., Scaramella R., Vettolani G., Zamorani G., 1992, *ApJ* 388, 9

Venturi T., Bardelli S., Morganti R., Hunstead R.W., 1997, *MNRAS* 285, 898

Venturi T., Bardelli S., Morganti R., Hunstead R.W., 1998, *MNRAS* 298, 1113

Willick J.A., Courteau S., Faber S.M., Burstein D., Dekel A., Strauss M.A., 1997, *ApJSS* 109, 333

Yahil A., 1985, in Richter O.G., Binggeli B. eds., *The Virgo cluster of galaxies*, ESO, München, p.359

Yentis D.J., Cruddace R.G., Gursky H., Stuart B.V., Wallin J.F., MacGillivray H.T., Collins C.A., 1992, in MacGillivray H.T., Collins C.A. eds., *Digitized Optical Sky Surveys*, Kluwer, Dordrecht, p.67

Vettolani G., et al., 1997, *A&A* 325, 954

Zucca E., Zamorani G., Scaramella R., Vettolani G., 1993, *ApJ* 407, 470

Zucca E. et al., 1997, *A&A* 326, 477

Table 2. Redshift data for the intercluster sample

PLATE 443						
α (2000)	δ (2000)	b_J	v	err	notes	
12 57 59.74	-29 32 43.9	17.88	31721	59		
12 58 19.96	-29 49 07.9	17.80	16879	69		
12 58 34.06	-29 26 12.7	17.78	25656	90		
12 58 39.13	-29 30 30.9	18.31	32048	171		
12 58 53.31	-29 19 49.8	18.66	32077	50		
12 59 22.10	-29 09 37.2	18.68	37148	106		
12 59 27.08	-29 49 01.1	17.25	14779	69		
12 59 46.95	-29 12 40.0	18.62	33036	145		
13 00 18.07	-29 44 04.1	17.56	17183	46		
13 00 35.04	-28 53 36.2	18.60	20412	14	emiss	
13 00 42.39	-29 51 18.2	17.54	18381	22	emiss	
13 00 46.28	-29 43 35.0	17.45	32185	103		
13 00 52.40	-29 38 06.5	17.80	28528	72		
13 00 55.25	-28 48 02.9	18.12	16301	146		
13 01 02.65	-28 15 58.9	18.56	40884	61		
13 01 07.29	-29 54 22.6	18.40	16529	78		
13 01 08.13	-28 59 58.2	18.17	19563	38		
13 01 14.71	-29 09 07.5	17.99	25461	84		
13 01 21.41	-28 34 23.2	18.35	22666	111		
13 01 23.49	-28 49 29.3	17.94	20113	36		
13 01 55.26	-29 07 14.1	18.78	20128	47		
13 01 56.28	-29 24 24.0	17.24	14821	66		
13 02 44.43	-28 50 12.2	18.05	26028	33		
13 02 45.77	-28 28 28.6	18.28	15304	146		
13 02 48.45	-28 45 15.7	18.64	23276	106		
13 02 57.03	-28 10 15.2	18.48	32293	65		
13 03 01.21	-28 42 07.1	18.55	31959	34		
13 03 05.59	-28 53 39.9	18.74	32412	56		
13 03 35.10	-28 14 02.4	18.62	20459	39		
13 04 00.45	-28 22 27.0	18.60	31361	32		
13 04 13.19	-29 31 20.1	18.24	14562	34	emiss	
13 04 27.74	-29 33 54.2	17.46	15496	10	emiss	
13 04 35.32	-29 05 31.9	18.79	40663	99		
13 04 35.39	-29 50 33.4	17.82	25772	32		
13 04 47.60	-28 22 17.5	18.79	14685	13	emiss	
13 04 49.98	-30 44 48.0	17.52	15698	35		
13 04 52.26	-28 36 13.6	18.61	14608	10	emiss	
13 04 55.94	-28 41 48.7	18.76	51978	107		
13 05 04.65	-29 11 12.1	18.03	31066	40		
13 05 08.80	-28 23 45.1	17.13	9427	64		
13 05 17.05	-30 52 10.0	18.66	39399	47		
13 05 17.99	-28 51 37.4	18.59	14998	10	emiss	
13 05 26.26	-28 58 13.9	18.43	31290	46		
13 05 27.80	-29 10 10.4	17.53	30365	81		
13 05 31.58	-29 54 00.2	18.07	20303	82		
13 05 31.93	-29 24 59.5	17.81	19655	23		
13 05 32.83	-28 24 39.2	18.09	22919	60		
13 05 35.15	-31 02 31.0	17.58	32296	81		
13 05 41.99	-30 57 11.3	17.50	29902	59		

Table 2. cont.

PLATE 443					
α (2000)	δ (2000)	b_J	v	err	notes
13 05 45.85	-29 08 40.0	17.56	31561	31	
13 05 47.53	-29 20 08.5	18.39	40349	64	
13 05 50.25	-30 36 09.9	18.73	31889	66	
13 05 50.52	-30 32 28.4	18.71	39476	119	
13 05 53.44	-28 38 56.0	18.66	31314	71	
13 05 53.98	-28 19 59.2	17.38	2266	35	emiss
13 05 54.06	-29 34 06.5	18.72	22248	37	
13 06 02.67	-29 11 47.7	17.06	15063	42	
13 06 20.00	-31 05 42.7	17.24	3783	97	
13 06 24.54	-28 42 56.1	18.54	48985	101	
13 06 24.57	-29 33 02.1	18.60	20478	64	
13 06 24.82	-28 14 12.8	17.93	38966	44	
13 06 24.82	-30 14 22.6	17.17	15490	105	
13 06 25.95	-29 26 49.9	18.76	40258	30	
13 06 27.09	-28 22 29.6	18.37	32462	52	
13 06 37.92	-29 38 22.1	17.18	19754	45	
13 06 47.48	-30 11 43.7	17.74	3443	107	
13 06 52.04	-28 56 04.8	17.48	21435	75	
13 06 55.60	-28 39 49.3	17.38	31893	89	
13 06 55.87	-28 53 13.7	18.67	26429	30	emiss
13 07 00.19	-28 18 24.8	18.61	6330	60	emiss
13 07 04.05	-29 08 00.6	18.64	35006	122	
13 07 06.70	-28 49 17.9	18.57	34453	33	
13 07 13.90	-30 35 15.6	17.14	3320	10	emiss
13 07 16.76	-28 30 49.1	17.33	22266	262	
13 07 24.04	-31 07 27.1	18.41	36270	46	
13 07 25.90	-30 22 21.7	18.11	22439	88	
13 07 35.84	-28 48 01.1	18.52	31765	37	emiss
13 07 37.01	-30 14 23.0	17.17	16919	107	
13 07 41.51	-30 52 58.6	18.66	39162	42	
13 07 51.58	-30 39 18.2	18.34	14210	45	
13 07 53.05	-29 16 40.4	18.21	31960	87	
13 07 55.93	-29 36 56.2	18.78	35135	27	
13 07 56.66	-28 18 43.1	18.65	40655	186	
13 07 58.35	-28 29 15.5	18.11	31823	30	
13 08 10.83	-28 34 25.5	17.81	32473	65	
13 08 12.01	-30 33 52.2	18.58	16928	10	emiss
13 08 20.29	-29 58 48.1	18.73	52649	42	
13 08 22.15	-29 23 40.7	18.70	30982	98	
13 08 29.51	-30 22 43.2	18.67	49202	135	
13 08 40.32	-28 35 56.6	18.44	32380	54	
13 08 49.52	-29 19 04.3	18.16	32544	66	
13 09 02.48	-30 46 34.7	17.21	11779	82	
13 09 06.31	-29 43 06.8	18.11	49031	50	
13 09 07.85	-30 37 47.2	18.11	9540	10	emiss
13 09 15.44	-28 42 47.9	18.14	32389	51	
13 09 19.59	-29 32 55.1	17.60	2886	39	
13 09 25.16	-29 18 01.3	17.44	14861	97	
13 09 33.38	-29 43 21.3	17.34	14948	10	emiss

Table 2. cont.

PLATE 443					
α (2000)	δ (2000)	b_J	v	err	notes
13 09 45.60	-29 12 42.2	18.00	23714	46	
13 09 47.44	-30 52 22.3	18.36	16908	21	
13 09 48.01	-28 22 06.8	17.78	14304	102	
13 09 49.11	-29 20 34.1	18.62	39497	43	
13 09 50.06	-29 31 00.1	18.05	14869	36	
13 09 54.92	-29 24 43.5	18.63	39219	54	
13 09 54.95	-30 00 59.2	17.09	16639	77	
13 09 56.38	-30 40 11.3	17.11	13409	117	
13 10 00.18	-30 26 54.0	18.69	31188	53	
13 10 06.42	-28 27 56.6	18.02	48899	52	
13 10 11.02	-28 19 47.5	18.39	35627	73	
13 10 19.83	-28 38 46.5	18.59	39393	95	
13 10 20.51	-29 01 15.9	18.62	39458	185	emiss
13 10 30.45	-30 38 07.4	18.16	9782	28	
13 10 34.46	-30 26 55.2	18.77	48245	47	
13 10 37.37	-29 01 12.0	18.38	32543	62	
13 10 42.20	-28 50 19.9	18.18	4650	10	emiss
13 10 42.53	-29 06 35.3	18.29	30853	45	
13 10 42.65	-30 50 27.3	18.30	35574	78	
13 10 44.32	-29 59 33.9	18.74	38941	31	
13 10 50.36	-28 42 25.2	18.62	36365	50	
13 10 53.75	-28 36 57.0	18.49	40191	37	
13 10 54.69	-30 23 31.1	18.62	22539	117	
13 10 56.85	-29 38 32.4	18.63	3229	16	
13 10 59.46	-29 58 16.7	18.76	38504	61	
13 11 02.03	-30 57 45.7	18.02	19827	10	
13 11 07.14	-29 16 11.2	18.52	49460	56	emiss
13 11 19.30	-29 49 37.8	18.57	52514	79	
13 11 22.03	-30 20 54.4	17.88	39861	72	
13 11 28.25	-28 56 18.8	18.58	49488	75	
13 11 29.59	-28 47 05.8	18.52	31992	39	
13 11 35.25	-29 48 14.6	17.78	30573	79	
13 11 45.55	-29 36 38.2	18.30	3529	88	
13 11 53.55	-30 16 04.1	18.19	24274	47	
13 12 08.62	-28 30 04.4	17.08	6969	51	emiss
13 12 18.11	-30 45 55.9	17.02	35933	35	
13 12 33.26	-30 47 31.2	17.75	35947	66	
13 12 40.15	-28 38 18.9	18.25	18321	138	
13 12 47.16	-28 25 22.9	18.23	23431	10	emiss
13 12 49.85	-31 21 31.8	17.49	20899	76	
13 12 59.19	-30 30 58.0	18.21	32540	62	
13 13 02.70	-30 25 53.9	18.69	9776	41	
13 13 07.82	-31 34 37.5	18.75	32331	38	
13 13 09.96	-30 41 47.9	17.83	23302	53	
13 13 15.62	-31 01 06.1	18.52	28809	130	
13 13 17.28	-28 30 23.2	18.66	38398	82	
13 13 30.74	-30 37 18.1	18.53	35966	57	
13 13 35.12	-31 48 20.8	17.68	14211	10	emiss
13 13 49.61	-31 57 17.6	18.12	15585	36	

Table 2. cont.

PLATE 443					
α (2000)	δ (2000)	b_J	v	err	notes
13 13 56.53	-32 06 11.9	18.02	34670	73	
13 13 57.70	-30 49 05.7	18.56	47538	65	
13 14 09.50	-31 35 37.5	17.69	31555	42	
13 15 26.60	-31 16 41.7	17.82	31812	25	
13 15 33.91	-31 20 13.5	18.42	31195	159	
13 15 40.58	-31 29 20.1	18.69	32782	39	
13 15 42.42	-31 25 22.9	18.44	38262	31	emiss
13 15 55.03	-31 42 51.0	17.50	4612	18	emiss
13 16 04.26	-31 51 11.2	18.76	38378	39	
13 16 19.67	-31 35 04.6	18.07	39184	36	

Table 2. cont.

PLATE 444					
α (2000)	δ (2000)	b_J	v	err	notes
13 14 23.51	-30 39 34.7	18.78	11998	10	emiss
13 14 24.78	-28 42 32.9	18.21	23693	153	
13 14 40.55	-30 41 55.9	18.76	36147	101	
13 14 43.03	-30 50 21.4	17.49	14728	101	
13 14 47.94	-30 24 11.3	18.78	30509	109	
13 14 51.06	-28 52 54.4	18.62	39765	51	
13 14 58.55	-30 16 21.4	18.19	21479	40	
13 15 07.98	-30 25 27.6	18.30	38954	34	
13 15 08.14	-30 57 02.6	18.27	29750	53	
13 15 18.05	-30 33 51.4	18.04	38888	41	
13 15 32.58	-30 20 19.2	18.21	25858	50	
13 15 51.53	-28 44 43.8	18.04	30333	177	
13 15 56.21	-28 29 05.0	17.22	13825	73	
13 15 59.98	-30 10 38.9	17.78	16101	10	emiss
13 16 01.64	-30 31 15.2	18.26	72825	46	
13 16 13.41	-30 48 18.1	18.11	25746	61	
13 16 17.09	-30 43 19.6	18.55	36348	74	
13 16 37.62	-30 55 26.2	17.75	30339	72	
13 16 41.01	-30 34 56.4	17.76	15297	42	emiss
13 17 04.19	-30 06 15.5	18.14	30360	67	
13 17 14.57	-30 44 26.5	17.35	21536	25	
13 17 22.58	-30 23 58.9	18.10	29991	50	
13 17 24.19	-28 30 37.1	18.10	15750	72	
13 18 00.56	-28 36 15.6	17.69	37396	39	
13 18 36.24	-28 27 41.9	18.04	37569	90	
13 19 24.70	-30 53 14.2	18.11	50426	23	emiss
13 19 30.12	-30 26 13.6	17.65	27762	37	
13 19 34.29	-30 29 10.2	18.40	29264	98	
13 19 40.72	-30 57 24.5	18.24	17968	40	
13 19 49.52	-30 21 02.4	18.32	34194	79	
13 20 31.94	-30 34 54.7	17.19	23387	71	
13 20 33.45	-30 32 13.1	18.48	35016	29	
13 20 39.99	-30 45 43.9	17.56	33082	42	
13 20 44.59	-30 20 43.7	18.00	4456	73	
13 20 47.66	-30 28 28.7	18.32	51391	37	
13 20 53.50	-30 12 24.3	17.85	39614	50	
13 21 08.11	-30 34 47.6	18.48	33156	37	
13 21 12.67	-29 53 27.2	17.29	14556	35	
13 21 24.11	-30 23 45.3	18.24	35484	48	
13 21 31.10	-30 45 54.6	18.32	49642	72	
13 21 35.10	-30 51 36.6	18.46	14492	27	emiss
13 21 36.18	-30 10 49.9	18.25	13854	54	
13 21 43.25	-29 39 05.8	17.71	23289	81	
13 21 53.22	-30 02 24.0	18.43	17154	20	emiss
13 21 55.42	-30 39 03.2	18.31	33141	35	
13 22 01.61	-29 56 54.0	17.84	34945	37	
13 22 02.15	-30 06 18.1	17.36	14800	76	
13 22 03.77	-29 35 11.8	17.00	9877	32	
13 22 17.92	-30 09 15.7	17.57	2489	10	emiss
13 22 22.28	-30 13 20.1	18.10	33261	58	

Table 2. cont.

PLATE 444					
α (2000)	δ (2000)	b_J	v	err	notes
13 22 33.65	-29 18 26.6	18.17	23032	90	
13 22 37.69	-30 25 12.6	17.77	25741	32	
13 22 44.86	-29 38 10.1	18.22	38377	83	
13 22 49.66	-30 06 51.8	18.14	4286	13	emiss
13 23 00.49	-29 18 32.9	17.77	14389	110	
13 23 20.83	-29 42 26.2	17.77	25798	61	
13 23 40.68	-30 00 51.8	18.62	9396	16	emiss
13 23 41.04	-29 33 24.4	18.68	22351	15	
13 23 49.77	-29 55 05.4	18.47	45851	132	
13 23 51.58	-29 21 41.2	18.50	22990	47	
13 24 24.97	-29 42 10.8	17.35	9845	158	
13 24 39.07	-30 40 50.7	17.91	14533	100	
13 24 48.35	-30 32 10.3	17.73	27469	54	
13 24 52.66	-30 36 28.4	18.53	27234	34	
13 24 55.63	-29 52 58.1	18.60	32789	90	
13 24 55.65	-30 44 51.4	17.57	27310	35	
13 24 55.76	-31 02 26.3	17.79	15658	101	
13 25 07.02	-29 59 50.1	17.75	14005	35	
13 25 07.08	-29 30 23.2	18.03	13925	26	
13 25 12.84	-30 20 21.4	17.77	4374	20	emiss
13 25 23.87	-29 49 58.9	18.09	14490	83	
13 25 23.95	-30 54 06.7	17.20	14171	144	
13 25 29.56	-30 45 34.9	17.70	43708	41	
13 25 35.52	-30 20 10.1	17.53	14050	13	emiss
13 26 34.06	-30 11 43.7	18.27	44029	76	
13 26 34.51	-30 47 32.6	18.51	14464	30	emiss
13 26 37.04	-31 00 22.7	17.95	15692	10	emiss
13 26 47.62	-30 28 59.9	17.34	9957	12	emiss
13 26 49.84	-30 37 56.6	17.90	14555	68	
13 27 00.37	-30 14 40.6	17.31	4224	10	emiss
13 27 29.06	-30 40 15.7	17.12	14136	31	
13 27 29.55	-30 33 31.4	17.13	14150	10	emiss
13 27 34.32	-30 23 03.3	18.26	13901	16	emiss
13 27 36.15	-30 58 47.7	17.92	13093	79	
13 28 03.33	-30 40 50.1	17.81	14996	55	
13 28 06.31	-30 34 49.8	17.80	14362	43	
13 28 23.03	-28 18 14.7	17.20	2053	20	emiss
13 28 26.44	-28 47 21.2	18.75	13366	31	emiss
13 28 28.63	-30 38 27.1	18.16	37888	30	
13 28 30.26	-30 46 55.2	18.33	37905	36	
13 28 41.59	-28 23 55.2	17.44	10792	96	
13 28 44.52	-30 34 09.1	18.76	38859	93	
13 28 46.53	-30 57 08.2	18.62	36656	72	
13 28 47.63	-30 21 23.9	18.20	27081	36	
13 28 58.94	-28 34 42.5	18.31	10722	95	
13 29 15.94	-28 26 06.9	18.13	9228	20	emiss
13 29 20.35	-30 46 37.7	17.97	14398	94	
13 29 31.15	-28 10 26.7	18.17	9793	24	
13 29 35.47	-28 57 09.6	18.22	42651	49	

Table 2. cont.

PLATE 444					
α (2000)	δ (2000)	b_J	v	err	notes
13 29 36.44	-30 32 15.7	18.08	14562	33	
13 29 44.29	-29 00 19.0	17.67	14694	25	
13 29 46.59	-30 48 06.3	18.26	43569	47	
13 29 56.15	-30 29 33.8	18.45	27398	133	
13 29 57.30	-28 14 27.1	18.15	9627	12	emiss
13 30 03.86	-31 05 41.5	17.75	13726	28	
13 30 05.47	-30 55 34.7	18.06	43402	37	
13 30 08.06	-28 37 17.5	18.76	34699	82	emiss
13 30 15.84	-30 36 17.4	17.03	15319	29	
13 30 19.55	-28 05 04.3	17.45	10205	39	
13 30 31.31	-30 19 29.7	18.01	37319	61	
13 30 31.84	-28 08 24.1	18.36	14195	27	emiss
13 30 42.61	-31 04 07.5	17.21	16085	93	
13 30 49.33	-30 19 23.6	18.36	40717	34	
13 30 53.17	-28 14 05.7	18.53	9055	86	
13 30 55.99	-29 00 51.8	18.15	2173	10	emiss
13 30 56.30	-28 04 56.2	17.72	5650	189	
13 31 05.59	-30 56 34.2	17.54	15781	34	
13 31 08.71	-30 40 44.8	17.77	26782	35	
13 31 15.84	-28 52 52.6	17.62	13940	150	
13 31 21.04	-30 45 54.9	17.64	22825	31	
13 31 21.93	-30 28 49.0	17.92	14506	28	
13 31 32.49	-30 55 13.1	17.53	14183	34	
13 31 37.96	-30 31 02.7	17.75	15003	102	
13 31 44.35	-28 28 38.9	18.12	44286	83	
13 31 59.37	-30 42 57.9	18.08	15176	102	
13 32 22.19	-28 37 14.7	18.43	13791	32	emiss
13 32 52.32	-28 37 52.4	17.24	34811	29	
13 33 09.99	-30 20 25.6	17.90	24342	23	emiss
13 33 13.22	-30 37 38.2	17.54	33162	66	
13 33 32.51	-30 12 00.2	17.10	14832	76	
13 33 35.80	-30 20 14.4	17.03	14698	38	
13 33 42.42	-28 29 43.0	17.70	13868	20	emiss
13 33 42.52	-30 28 09.9	17.14	10877	20	
13 33 42.97	-30 08 58.0	18.54	47984	94	
13 33 48.65	-28 15 25.1	18.60	9721	46	
13 33 55.53	-30 42 28.7	18.34	22400	77	
13 34 01.58	-30 49 26.5	18.26	37269	67	
13 34 10.74	-30 57 27.0	18.09	13635	10	emiss
13 34 19.45	-28 52 34.1	17.25	22656	37	
13 34 24.56	-28 41 11.1	18.33	34534	59	
13 34 38.57	-28 35 36.0	18.49	35852	29	emiss
13 34 40.86	-30 13 00.4	17.37	10995	58	
13 34 42.90	-30 26 02.7	17.46	15132	82	
13 35 04.11	-28 58 23.5	18.71	13262	81	
13 35 09.30	-30 11 59.1	18.25	35140	100	
13 35 19.88	-30 18 58.5	17.42	22488	10	emiss
13 35 22.59	-30 49 22.7	18.35	39636	53	
13 35 46.54	-29 00 32.7	18.24	45965	28	
13 35 52.58	-30 47 27.2	18.20	22514	58	

Table 2. cont.

PLATE 444						
α (2000)	δ (2000)	b_J	v	err	notes	
13 35 53.92	-28 17 58.4	17.18	13513	11	emiss	
13 35 55.36	-30 33 11.1	17.29	4187	27	emiss	
13 35 59.05	-30 22 34.4	18.28	13840	10	emiss	
13 36 05.99	-28 26 08.7	18.37	35100	29		
13 36 19.57	-28 56 08.3	17.75	14439	114		
13 36 23.50	-28 45 01.2	18.70	46416	118		
13 36 29.19	-28 27 47.6	18.21	35020	41		
13 36 30.31	-28 34 48.5	17.77	35723	36		
13 36 37.84	-30 30 55.8	17.40	22269	111		
13 36 41.41	-30 25 18.6	17.00	11319	45		
13 36 55.64	-28 40 31.3	18.66	46502	139		

Table 2. cont.

PLATE 509						
α (2000)	δ (2000)	b_J	v	err	notes	
13 25 10.03	-24 30 24.9	18.43	32843	40		
13 25 31.76	-24 25 03.7	17.54	22802	66		
13 25 31.96	-24 18 56.9	17.74	24183	74		
13 25 36.96	-25 46 45.1	17.13	9538	181		
13 25 40.35	-25 57 45.1	18.75	19718	14	emiss	
13 25 42.43	-25 53 12.4	17.41	18019	36		
13 25 43.19	-25 36 06.5	18.65	27159	187		
13 25 45.61	-24 44 10.7	17.48	10086	77		
13 25 49.54	-24 34 13.0	17.43	12123	30	emiss	
13 25 52.99	-24 12 50.0	18.55	12336	18	emiss	
13 26 01.68	-26 08 12.2	18.34	26637	43		
13 26 17.94	-25 37 22.8	18.18	12514	10	emiss	
13 26 20.15	-24 13 18.3	18.40	41508	94		
13 26 22.52	-25 56 25.7	18.16	31868	42		
13 26 25.60	-25 24 45.1	17.63	7716	42		
13 26 43.87	-25 18 42.4	18.33	50105	82		
13 26 44.62	-24 17 48.2	17.75	9821	10	emiss	
13 26 45.49	-25 44 56.4	18.31	15436	31		
13 26 47.44	-26 10 41.1	18.31	39962	43		
13 26 47.98	-24 39 42.1	18.02	13483	32		
13 26 54.01	-24 46 27.1	18.36	13782	58		
13 26 56.43	-23 18 08.0	17.62	13633	42		
13 26 56.68	-24 16 11.9	17.66	13337	36		
13 27 04.23	-24 30 18.6	17.46	13502	54		
13 27 06.47	-25 27 46.6	17.51	13712	44		
13 27 09.10	-24 26 07.3	18.51	13723	32		
13 27 15.08	-24 01 47.0	17.65	34321	49		
13 27 32.39	-25 35 13.3	18.59	9075	15	emiss	
13 27 36.02	-23 34 06.5	17.49	9745	41		
13 27 40.01	-24 12 42.7	17.19	9940	25		
13 27 43.55	-24 45 05.1	18.45	32693	134		
13 27 46.98	-25 18 16.4	17.50	12955	28		
13 27 50.62	-24 56 06.4	17.58	27239	38		
13 27 51.87	-24 03 37.4	18.25	9338	95		
13 27 57.53	-25 40 14.3	17.95	11392	76		
13 27 58.62	-26 09 59.1	18.76	32308	133		
13 28 01.56	-24 14 32.3	18.02	13296	26		
13 28 02.38	-26 02 37.5	18.26	36880	148		
13 28 14.09	-23 39 27.1	18.34	41532	70		
13 28 14.56	-24 37 00.3	17.16	13360	34		
13 28 16.78	-24 21 10.7	17.93	12749	30		
13 28 18.22	-24 42 34.6	17.40	14149	52		
13 28 19.32	-25 57 42.8	18.53	30767	185		
13 28 21.34	-25 28 35.7	17.27	13635	31		
13 28 22.50	-24 28 19.9	17.25	13486	34		
13 28 32.49	-24 00 30.4	17.17	12758	61		
13 28 38.58	-26 04 27.8	18.02	13473	41		
13 28 45.81	-24 10 22.9	18.71	12700	42		
13 28 46.29	-25 37 00.4	17.70	12649	10	emiss	
13 29 12.54	-25 32 34.0	17.57	13060	94		

Table 2. cont.

PLATE 509					
α (2000)	δ (2000)	b_J	v	err	notes
13 29 25.19	-25 52 00.7	17.94	27692	33	
13 29 25.46	-23 39 34.8	18.17	5422	10	emiss
13 29 26.77	-23 44 23.6	18.74	23057	48	
13 30 07.83	-25 09 59.0	17.43	10448	50	
13 30 13.67	-25 05 33.2	18.19	32264	81	
13 30 29.81	-25 17 51.1	18.23	38231	57	
13 30 42.02	-25 21 25.1	17.28	13445	94	
13 30 50.03	-25 26 05.4	17.61	13556	42	
13 31 02.04	-24 57 39.0	18.62	32226	91	
13 31 21.56	-25 23 36.9	17.73	27941	34	
13 31 48.40	-24 56 01.2	17.43	7860	63	
13 32 04.35	-25 00 03.5	18.37	38543	250	
13 32 35.44	-24 49 28.9	17.64	14880	123	
13 32 43.60	-25 16 34.5	18.40	34941	64	
13 32 45.92	-25 24 11.8	18.45	35690	70	
13 32 55.69	-25 09 49.8	17.14	12429	72	
13 32 58.67	-25 23 29.0	18.68	71679	71	
13 33 43.10	-25 02 42.3	17.74	19161	31	
13 34 45.65	-24 41 02.6	18.61	36344	46	
13 34 45.99	-24 45 18.7	18.65	19208	13	emiss
13 34 48.52	-26 45 37.4	18.46	10914	111	
13 34 55.38	-27 07 15.0	17.67	10533	67	
13 34 56.82	-27 00 59.1	17.44	9746	58	emiss
13 34 57.99	-24 22 28.8	18.29	38124	64	
13 35 05.00	-24 56 13.2	18.63	37110	31	
13 35 05.91	-27 14 32.7	18.15	10282	42	emiss
13 35 20.57	-25 47 55.3	18.37	46970	183	
13 35 36.18	-25 40 01.0	17.02	31094	201	
13 35 43.17	-27 11 13.6	18.27	11319	18	emiss
13 35 51.92	-25 57 38.2	18.44	28385	49	emiss
13 35 52.58	-24 41 08.4	17.56	20177	74	
13 35 55.62	-24 19 02.6	17.00	19596	25	emiss
13 35 59.00	-24 07 22.9	17.90	37849	82	
13 36 08.10	-25 27 23.3	17.89	32532	45	
13 36 21.74	-26 55 41.1	17.93	36770	63	
13 36 22.53	-26 46 45.3	17.78	35672	62	
13 36 24.27	-26 06 30.0	18.21	20469	88	
13 36 26.89	-27 14 07.7	17.26	13448	97	
13 36 29.28	-25 24 13.8	18.30	39324	151	
13 36 36.63	-26 32 29.5	17.77	6865	33	
13 36 37.89	-27 03 17.7	17.74	13443	85	
13 36 40.65	-26 57 00.6	18.52	36272	67	
13 36 42.14	-24 22 47.9	18.46	37480	69	
13 36 54.89	-24 40 18.6	17.63	4762	42	
13 37 07.34	-24 10 04.0	18.32	36516	43	
13 37 13.48	-26 58 26.1	18.61	22094	53	
13 37 21.91	-25 48 14.2	18.62	25195	160	
13 37 33.22	-27 15 19.9	18.00	33022	36	
13 37 37.41	-25 19 11.7	18.10	35883	135	
13 37 38.86	-24 40 54.9	18.48	6752	10	emiss

Table 2. cont.

PLATE 509					
α (2000)	δ (2000)	b_J	v	err	notes
13 37 41.61	-24 29 16.6	18.16	20013	53	
13 37 46.97	-24 15 04.0	18.24	32058	26	
13 37 55.87	-26 41 57.8	17.79	32287	121	
13 38 00.39	-25 53 16.4	18.25	30775	73	
13 38 08.45	-24 29 49.4	18.68	42571	30	
13 38 21.49	-25 23 11.4	17.77	35326	99	
13 38 22.69	-25 37 00.8	18.13	37322	69	
13 38 37.96	-27 07 12.1	17.15	4725	24	emiss
13 38 39.73	-26 45 53.7	18.06	26857	71	
13 41 55.79	-24 31 52.5	18.66	36573	68	
13 41 56.94	-24 23 01.0	17.41	16897	123	
13 42 13.25	-24 09 25.5	18.02	37697	97	
13 42 16.89	-24 36 15.8	17.85	29093	64	
13 42 31.15	-24 47 26.7	17.59	18330	101	
13 42 32.70	-24 31 06.0	18.71	36609	73	
13 42 47.60	-24 27 50.5	18.51	19372	12	emiss
13 43 25.14	-25 01 31.1	17.46	14530	114	
13 43 32.11	-24 33 54.0	17.00	36728	34	
13 43 39.07	-24 20 12.2	17.40	6913	50	
13 43 53.74	-24 53 19.6	18.11	14341	70	
13 44 20.97	-24 50 53.4	17.70	43024	91	
13 44 22.65	-24 45 29.2	18.57	37839	165	
13 44 37.25	-24 20 14.2	18.55	6369	92	
13 44 44.42	-24 42 58.3	18.60	36252	165	
13 44 55.45	-24 37 30.0	18.17	27656	28	